Electronic Supplementary Material (ESI) for Polymer Chemistry.

Supporting Information

Multimesophase Transitions of Main-Chain Liquid Crystalline Copolymers with Strictly Alternating Fluorocarbon Chains

Enjie He, Kai Tu, Jiannan Cheng, Huanjun Lu, Lifen Zhang*, Zhenping Cheng*, Xiulin Zhu*

Suzhou key Laboratory of Macromolecular Design and Precision Synthesis, Jiangsu Key Laboratory of Advanced Functional Polymer Design and Application; State and Local Joint Engineering Laboratory for Novel Functional Polymeric Materials; College of Chemistry, Chemical Engineering and Materials Science, Soochow University, Suzhou 215123, China.

E-mail: chengzhenping@suda.edu.cn (Z. P. Cheng), zhanglifen@suda.edu.cn (L. F. Zhang) or huanjunlu@suda.edu.cn (H. J. Lu)

1. Supplementary Tables and Figures

Table S1. Synthesis of F_nH_m(I)MH_m(I) series liquid crystalline copolymers[a]

Copolymer	R	Solvent (mL)	Time (h)	$n_{(A)}$ (mmol)	[b]$M_{n,GPC}$ (kDa)	[b]M_w/M_n
F_4H_6(I)MH_6(I)	1:1:0.02:0.5	Dioxane/Methanol (3/1)	96	0.5	9.9	1.84
F_4H_7(I)MH_7(I)	1:1:0.02:0.5	Dioxane/Methanol (3/1)	96	0.5	11.5	1.98
F_6H_6(I)MH_6(I)	1:1:0.02:0.5	DMC/Acetonitrile (3/1)	3	0.3	8.8	1.82
F_6H_7(I)MH_7(I)	1:1.2:0.02:0.5	Dioxane/Methanol (3/1)	20	0.5	12.6	1.94
F_6H_8(I)MH_8(I)	1:1:0.02:0.5	Dioxane/Methanol (4/3)	16.5	0.5	9.9	1.42
F_6H_9(I)MH_9(I)	1:1.2:0.02:0.5	Dioxane/Methanol (3/1)	11.5	0.5	12.0	1.81
F_8H_6(I)MH_6(I)	1:1:0.02:0.5	Dioxane/Methanol (3/1)	72	0.5	14.8	1.68
F_8H_7(I)MH_7(I)	1:1:0.02:0.5	Dioxane/Methanol (3/1)	72	0.5	13.7	1.90

[a]Polymerization conditions: R = $[A]_0$:$[B]_0$:$[Ru(bpy)_3Cl_2]_0$:$[AsAc\text{-}Na]_0$, A = $I(CF_2)_nI$, B = H_mMH_m, under irradiation with blue LED light (λ_{max} = 458 nm, 4.9 mW cm^{-2}), T = 25 ^{o}C. [b]Molecular weights and molecular weight distributions were determined by GPC using PS as the standard in DMF (with 0.1 wt.% of LiBr).

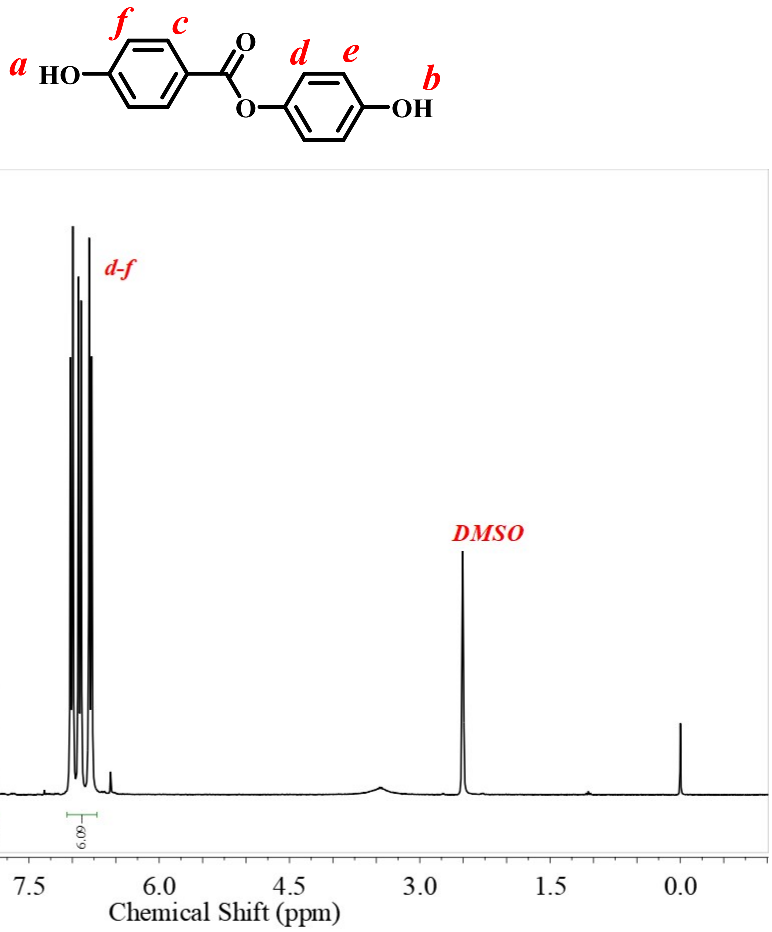

Figure S1. ^{1}H NMR spectrum of HPHB.

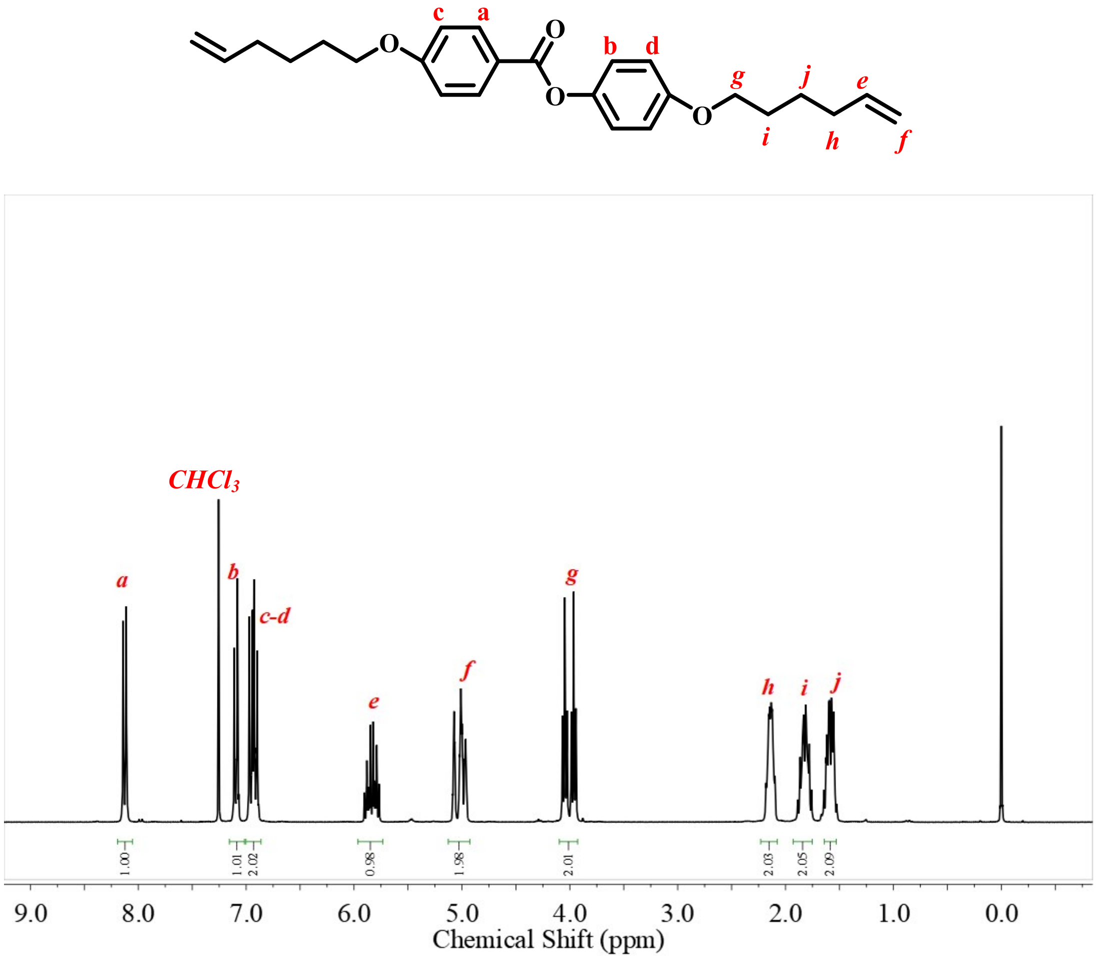

Figure S2. ^{1}H NMR spectrum of H_6MH_6.

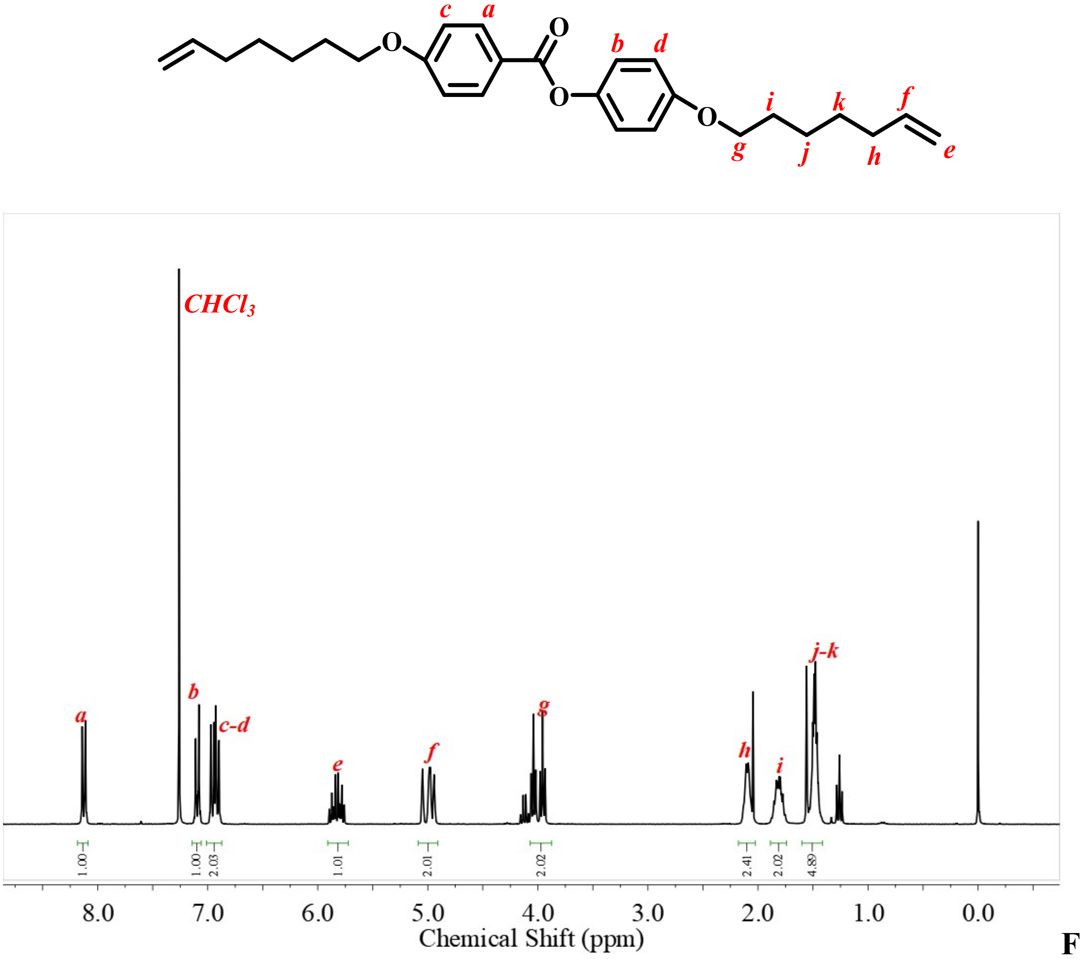

Figure S3. ^{1}H NMR spectrum of H_7MH_7.

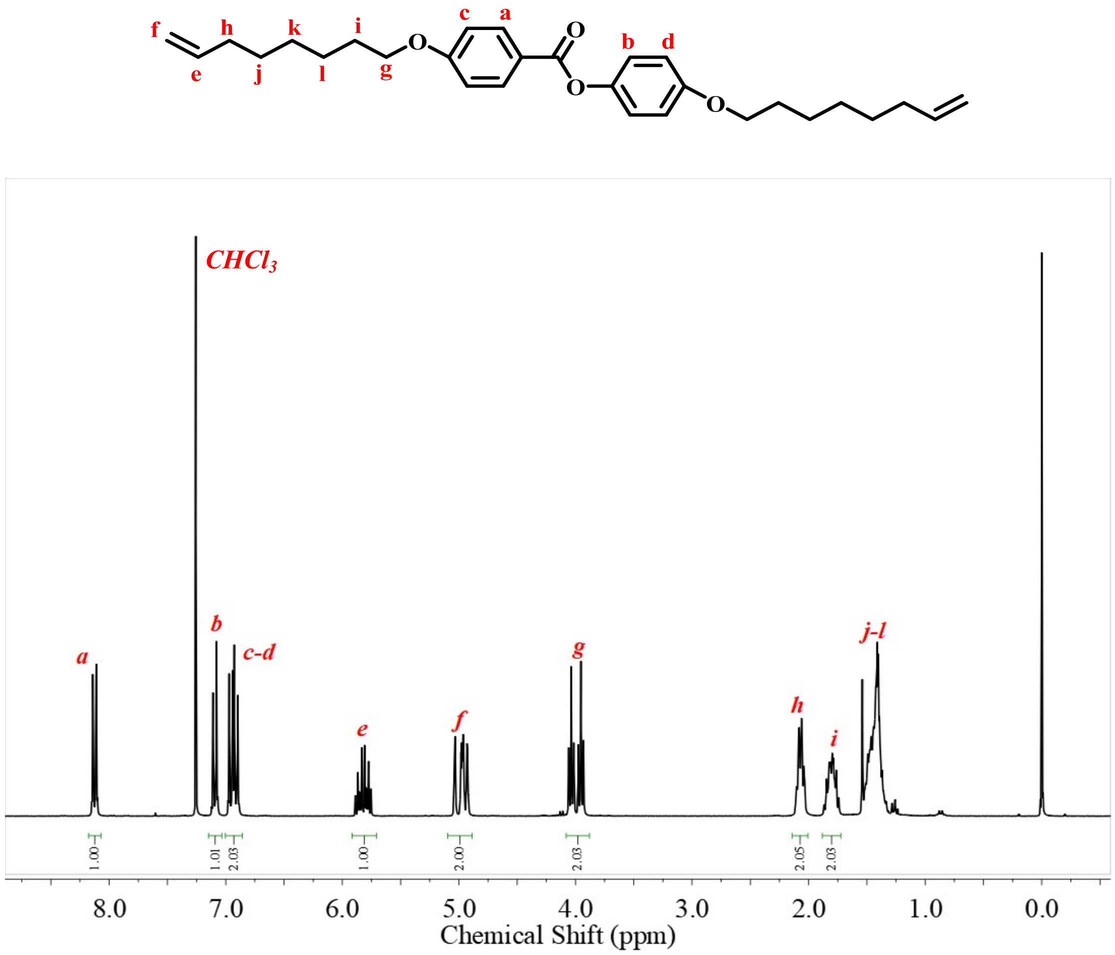

Figure S4. ^{1}H NMR spectrum of H_8MH_8.

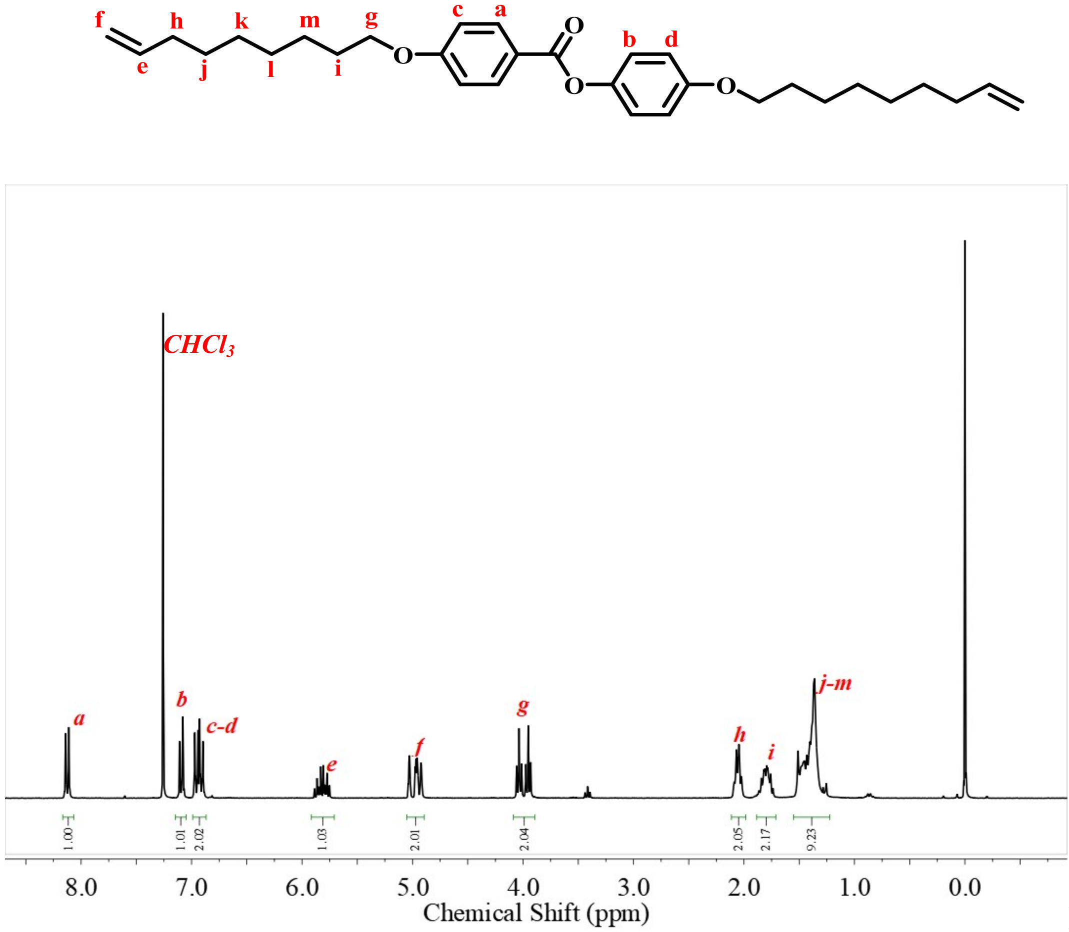

Figure S5. ^{1}H NMR spectrum of H$_9$MH$_9$.

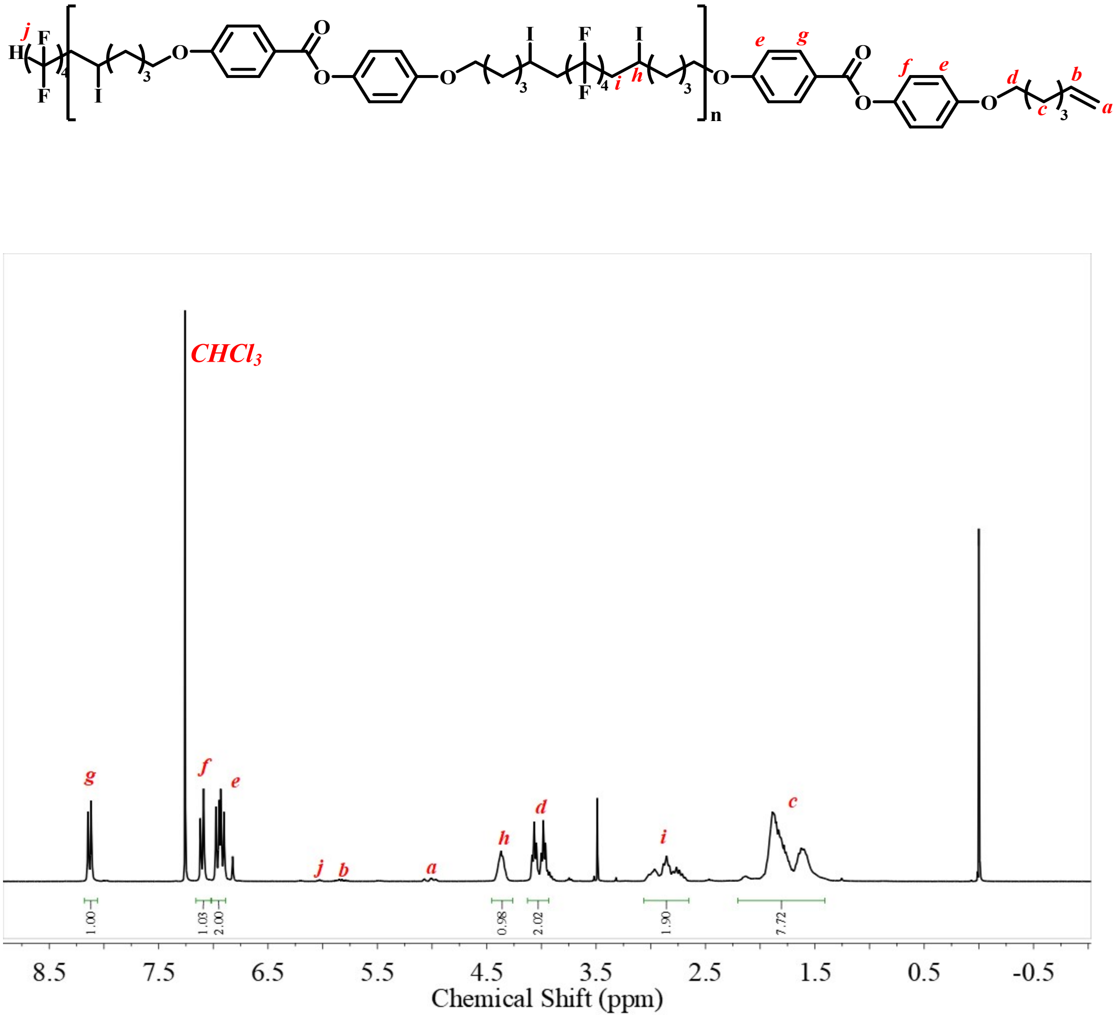

Figure S6. ^{1}H NMR spectrum of $F_4H_6(I)MH_6(I)$.

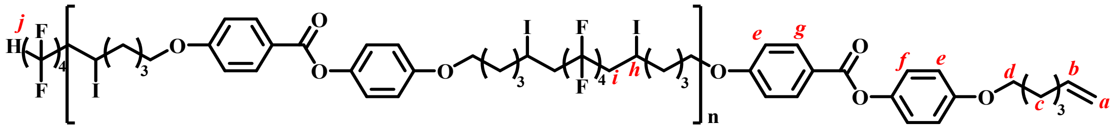

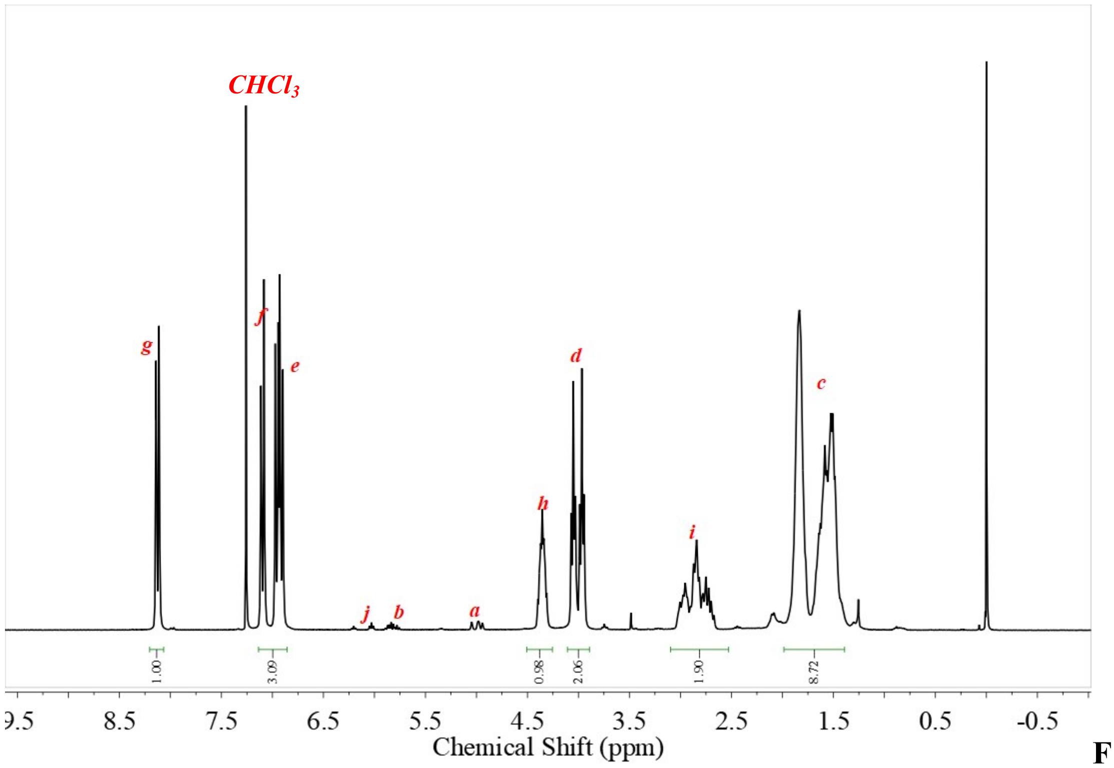

F

igure S7. ^{1}H NMR spectrum of $F_4H_7(I)MH_7(I)$.

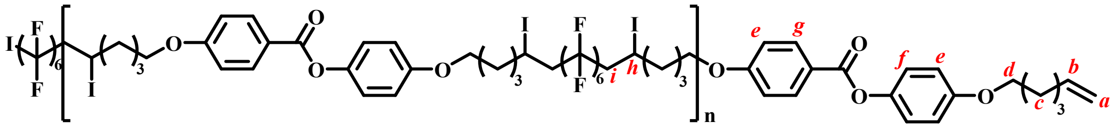

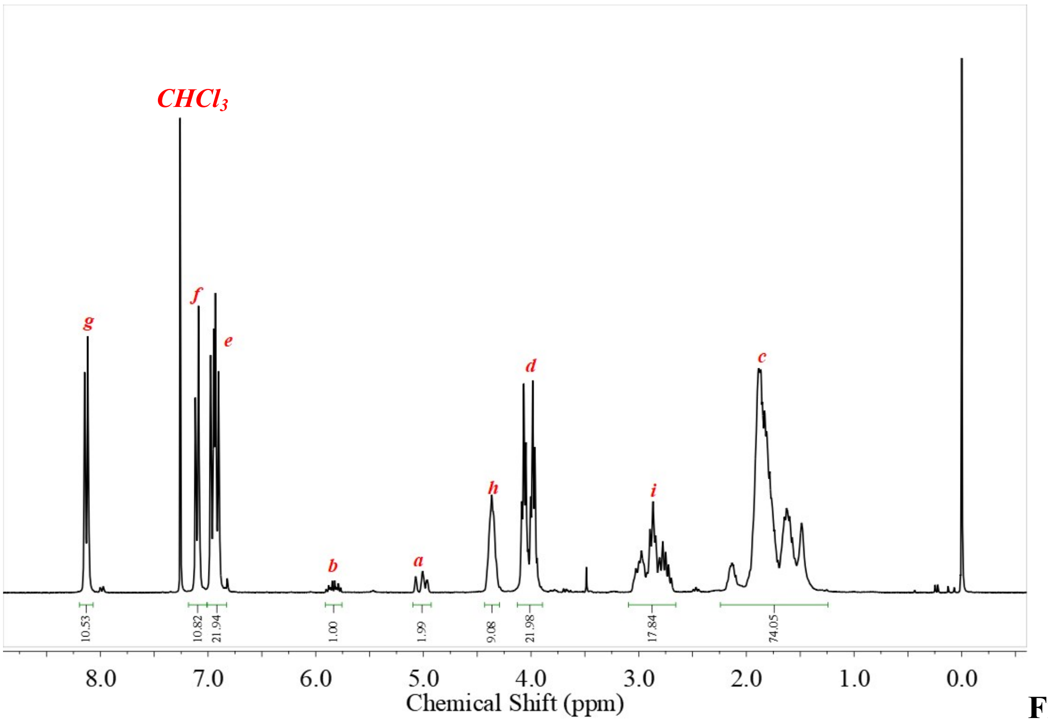

Figure S8. ^{1}H NMR spectrum of $F_6H_6(I)MH_6(I)$.

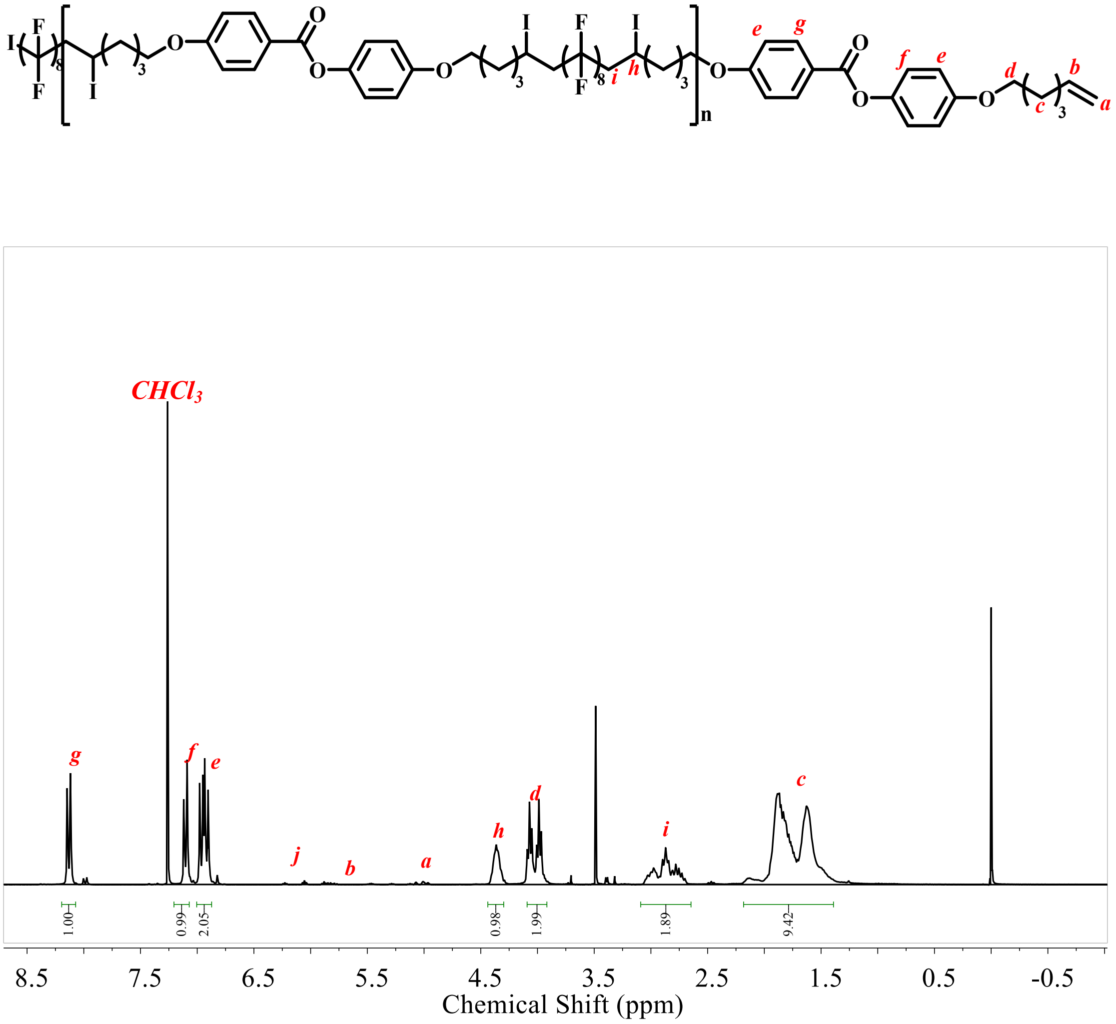

Figure S9. ^{1}H NMR spectrum of $F_8H_6(I)MH_6(I)$.

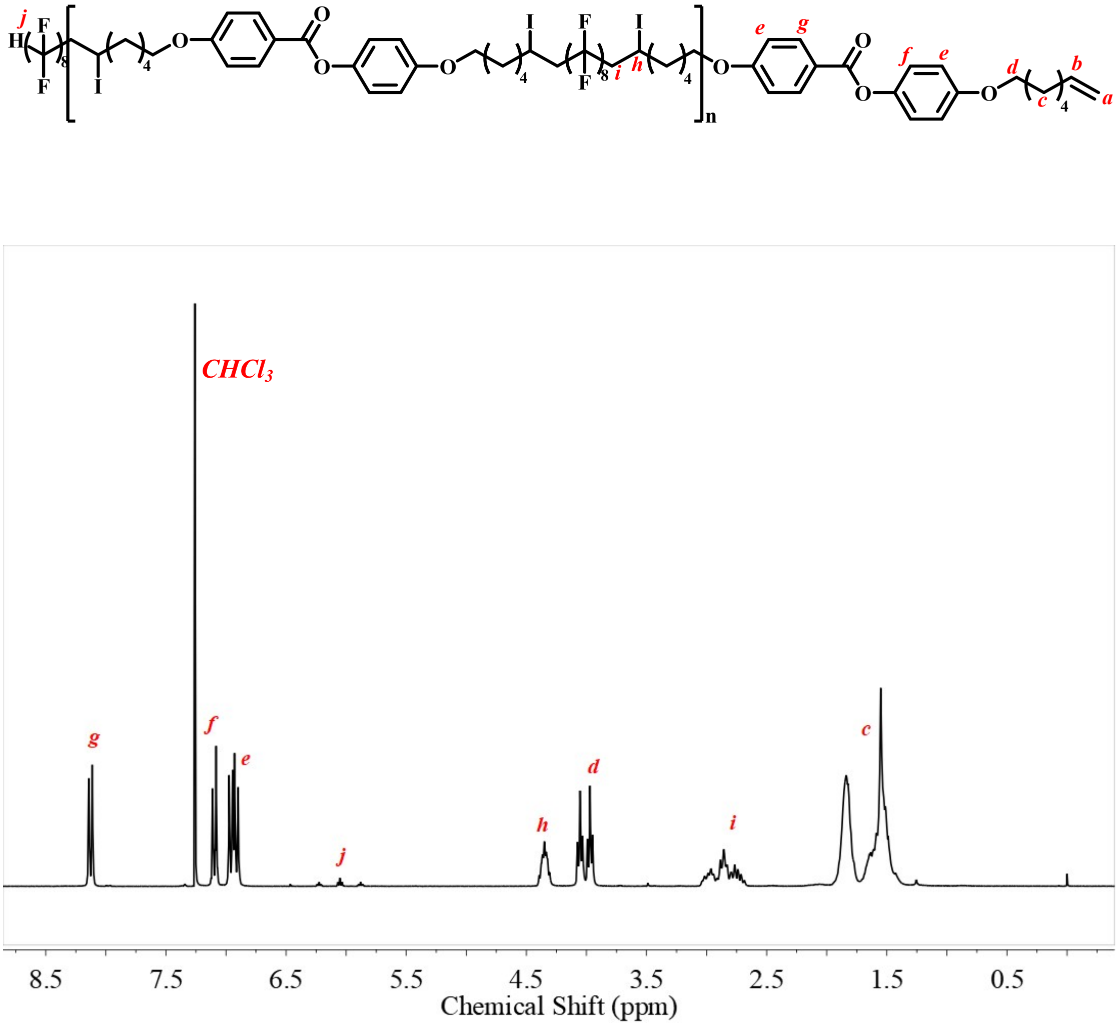

Figure S10. ^{1}H NMR spectrum of $F_8H_7(I)MH_7(I)$.

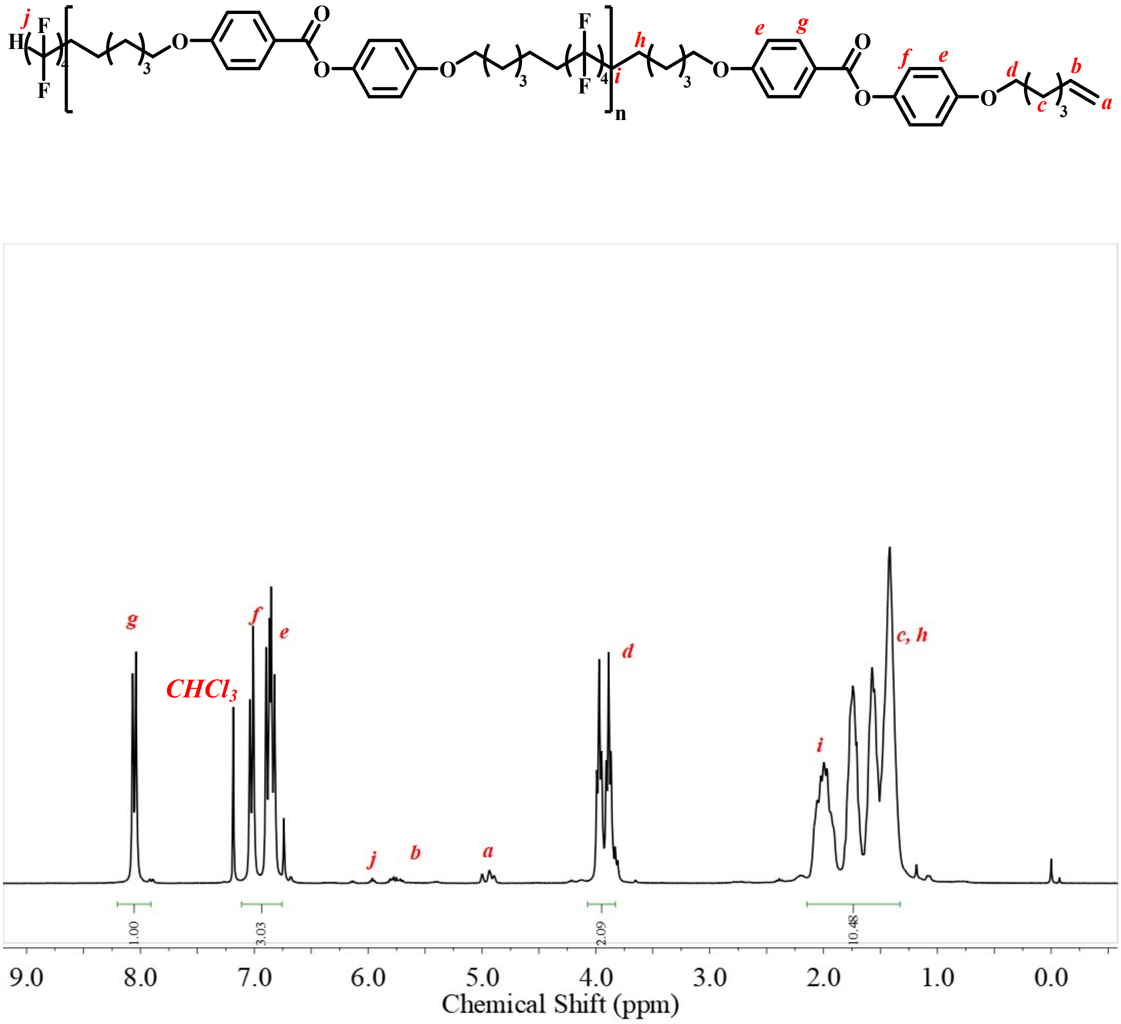

Figure S11. ^{1}H NMR spectrum of $F_4H_6MH_6$.

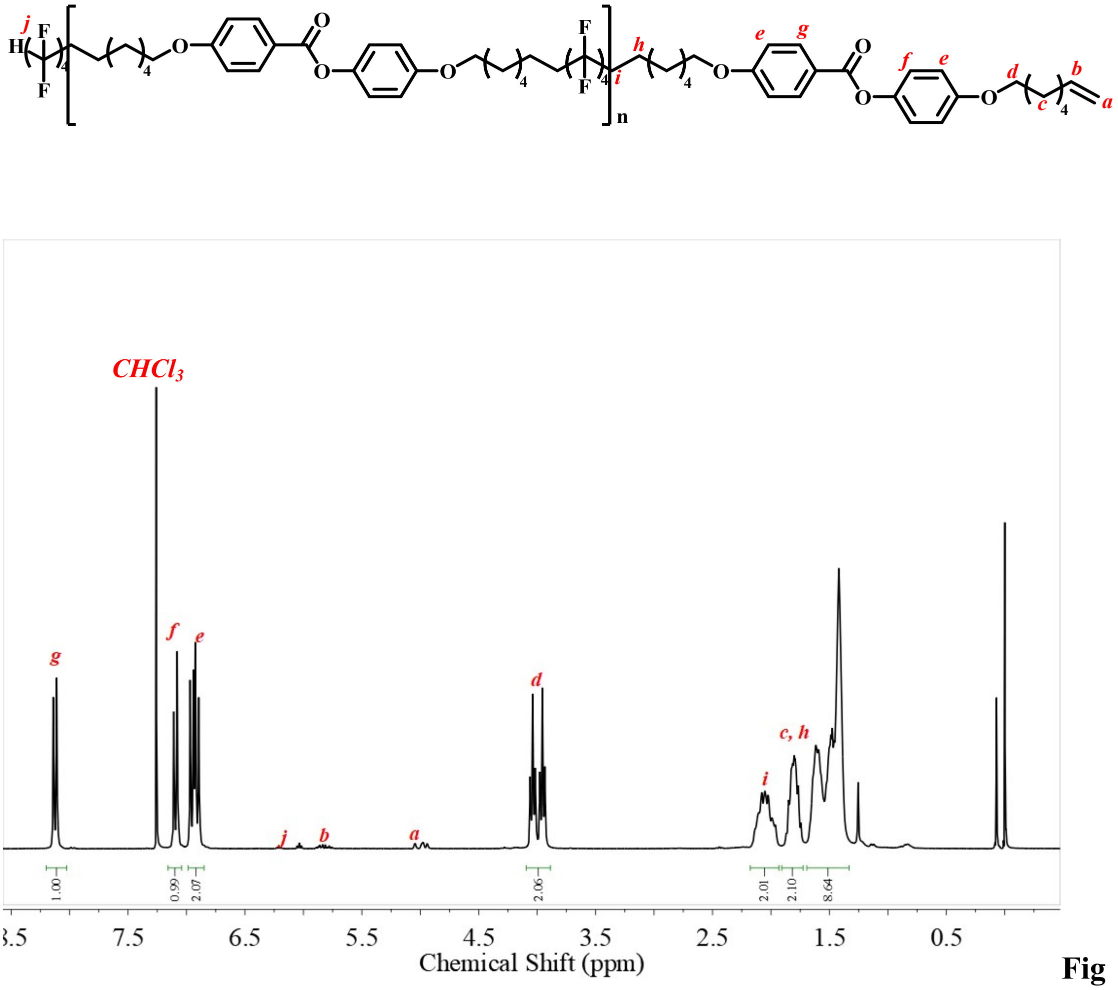

Figure S12. ^{1}H NMR spectrum of $F_4H_7MH_7$.

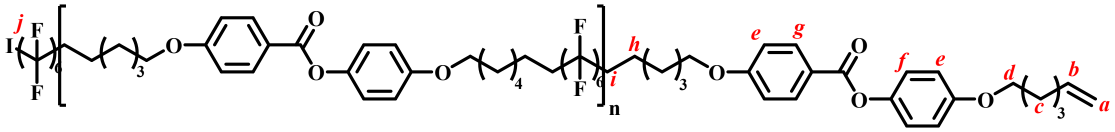

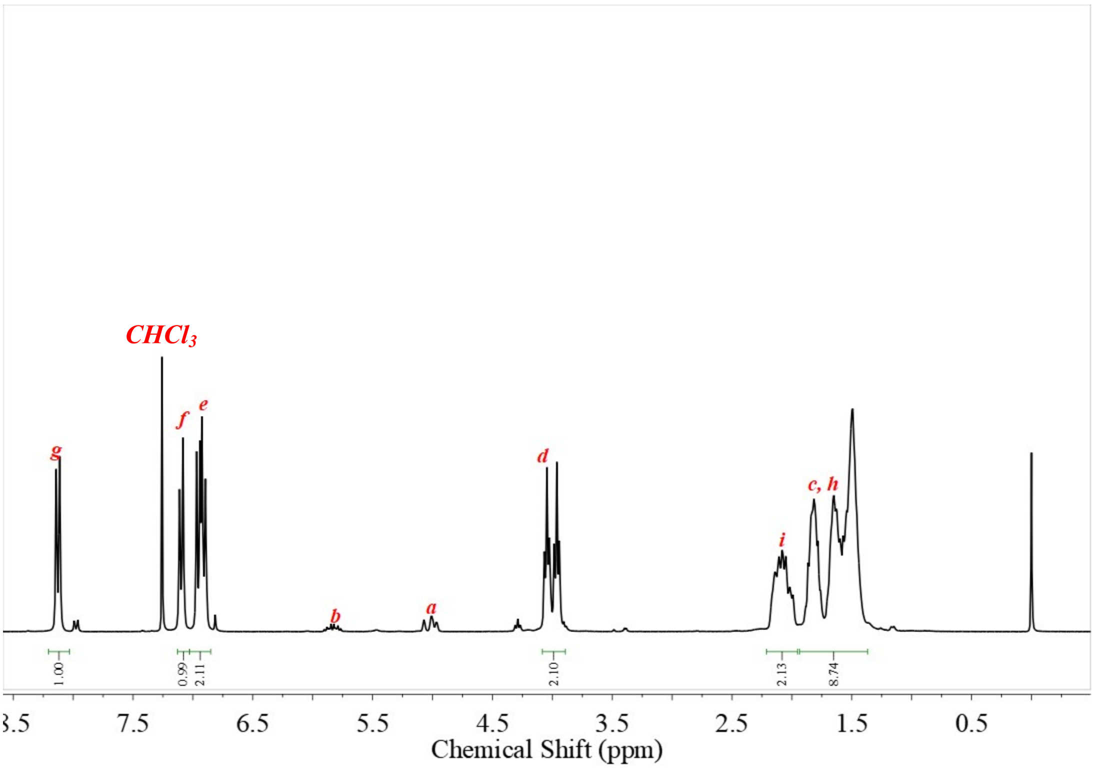

Figure S13. ^{1}H NMR spectrum of $F_6H_6MH_6$.

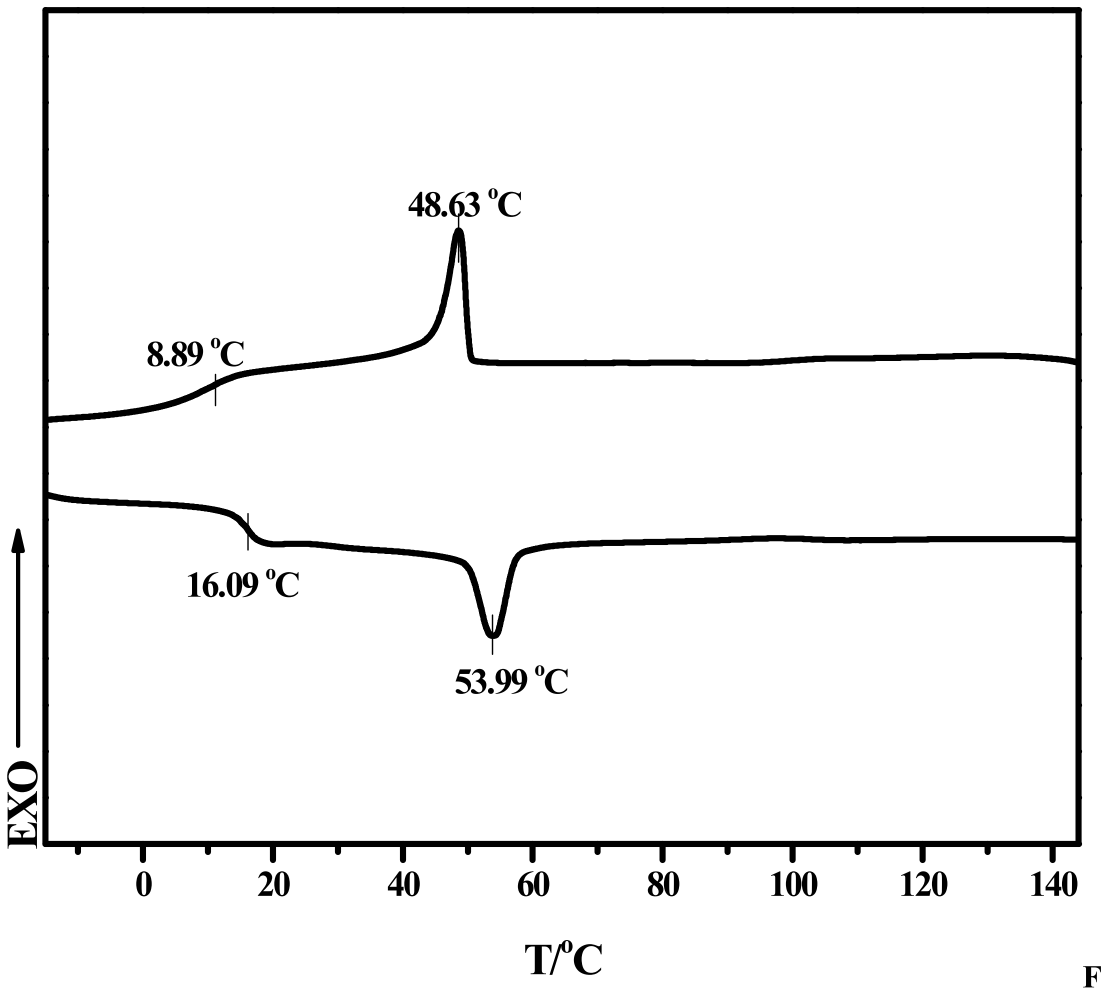

F

igure S14. DSC curve of $F_4H_6(I)MH_6(I)$ obtained at a heating/cooling scanning rate of 10 °C min^{-1}.

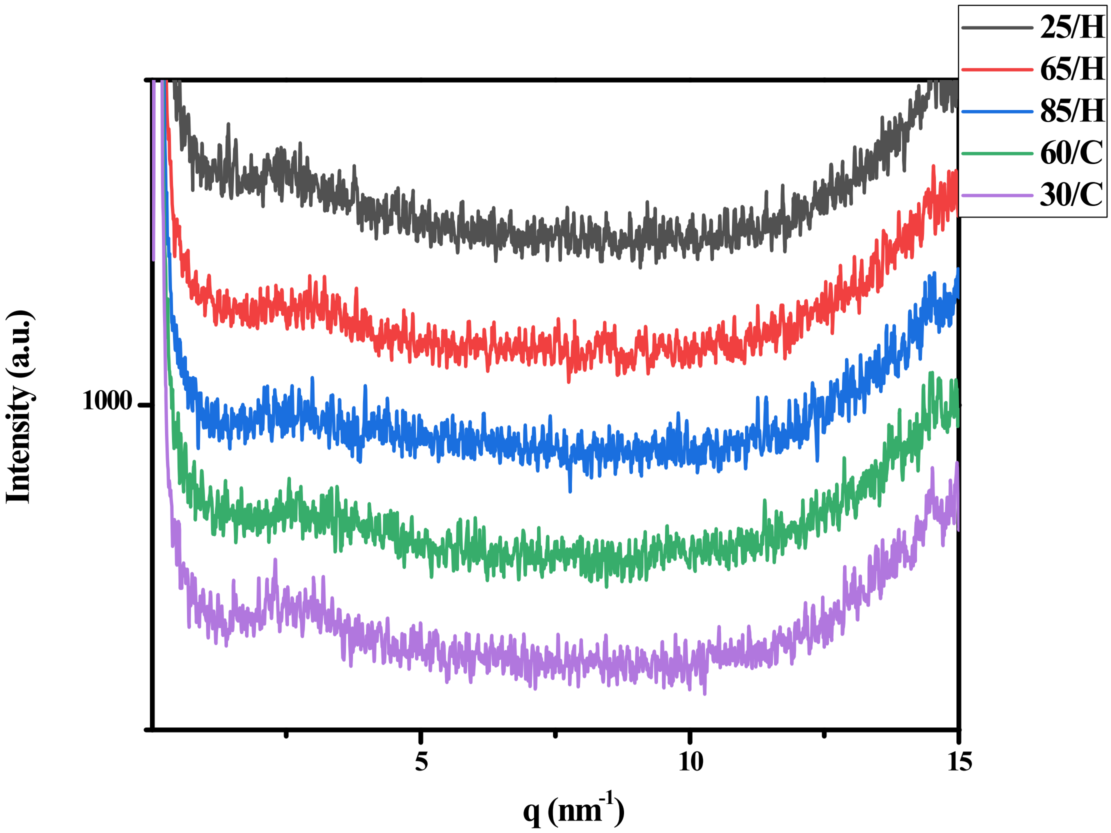

Figure S15. SAXS spectra of $F_4H_6(I)MH_6(I)$ at different temperatures after being annealed. 25/H means 25 ^{o}C/heating; similarly, 60/C means 60 ^{o}C/cooling.

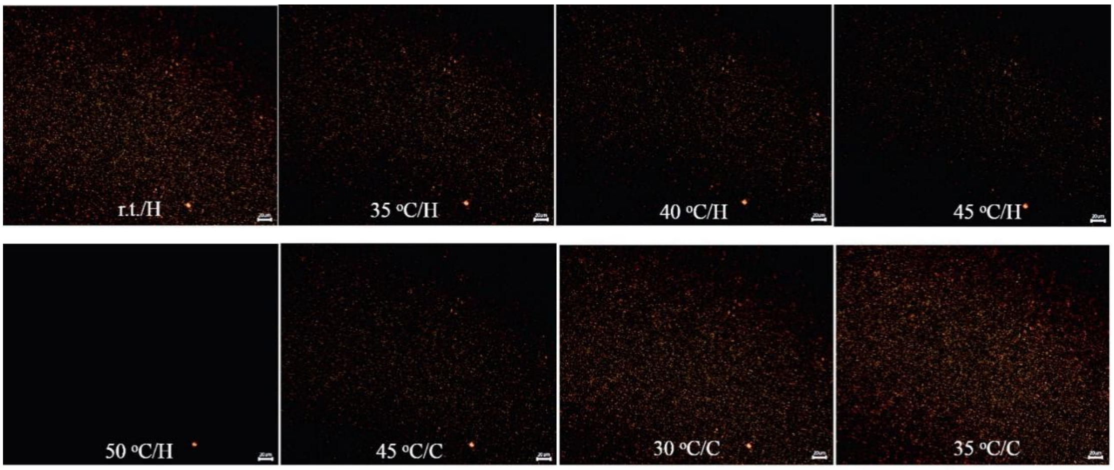

Figure S16. POM images of $F_4H_6(I)MH_6(I)$ at different temperatures.

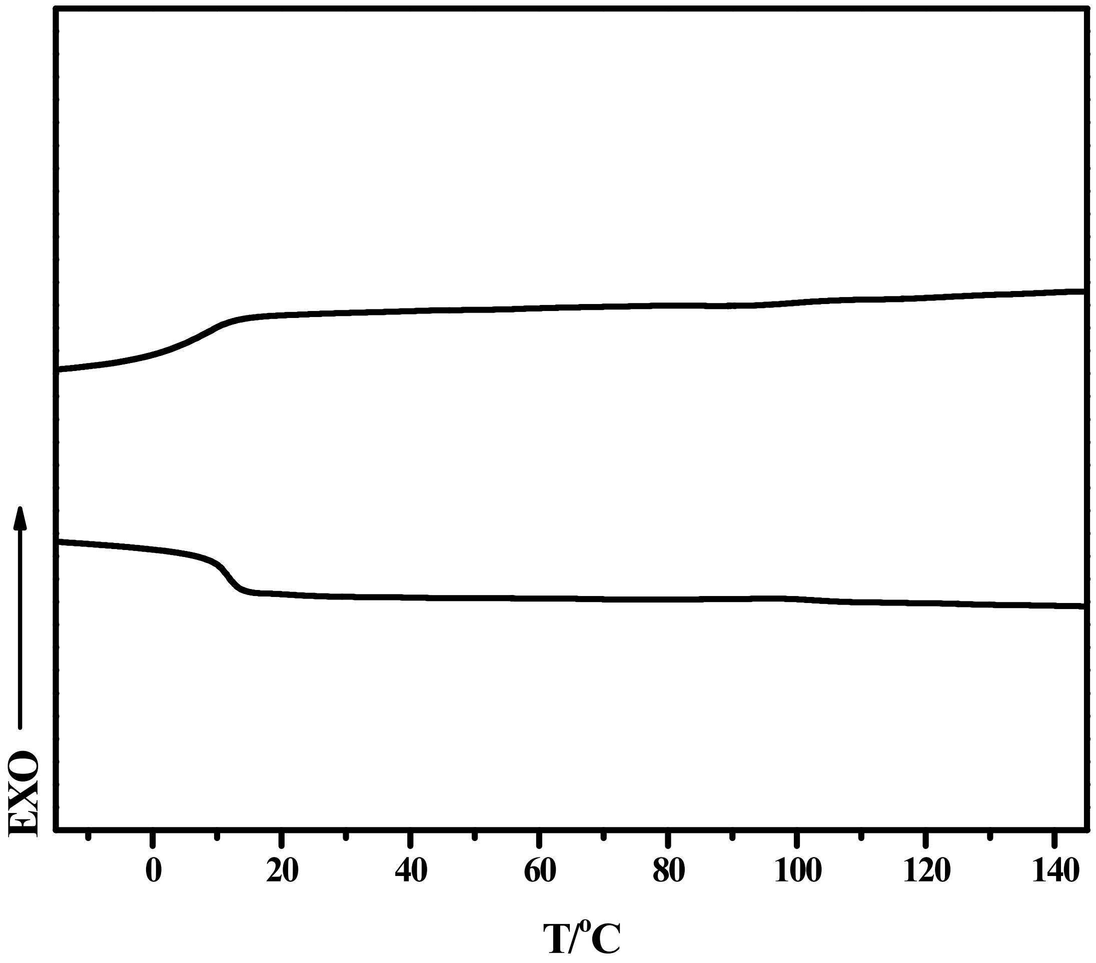

Figure S17. DSC curve of $F_4H_7(I)MH_7(I)$ obtained at a heating/cooling scanning rate of 10 °C min^{-1}.

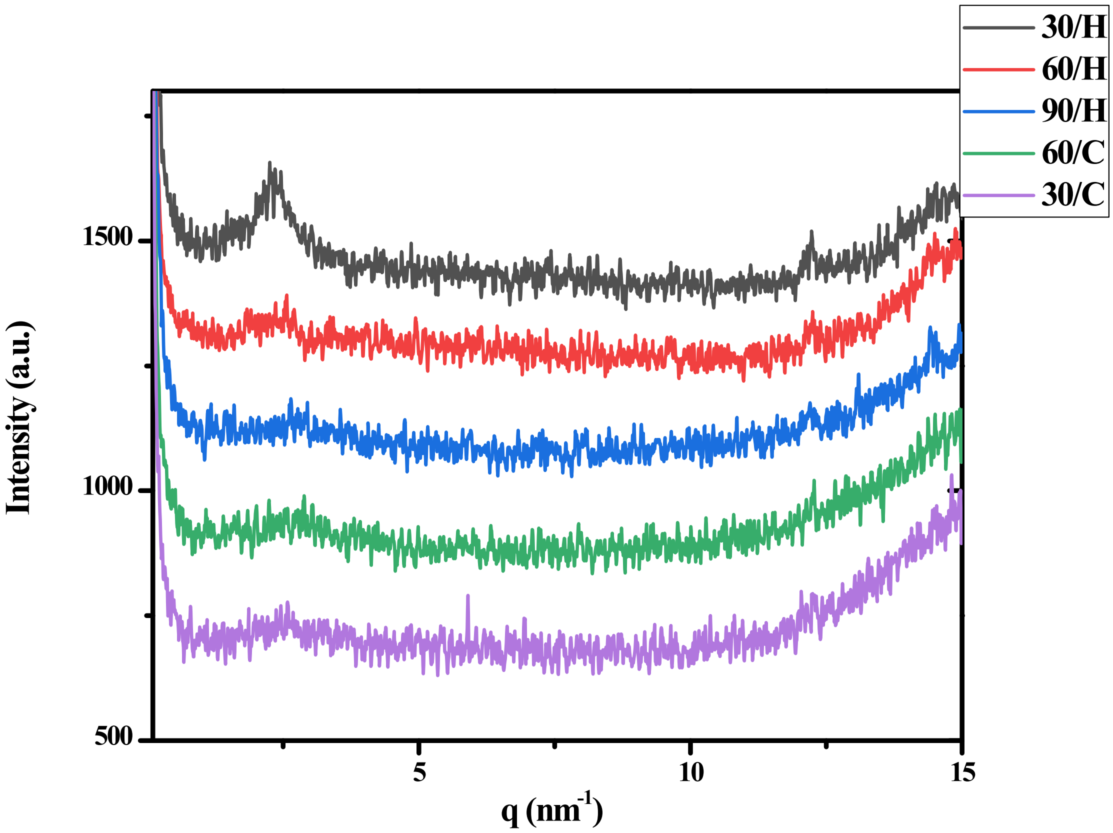

Figure S18. SAXS spectra of F_4H_7(I)MH_7(I) at different temperatures after being annealed.

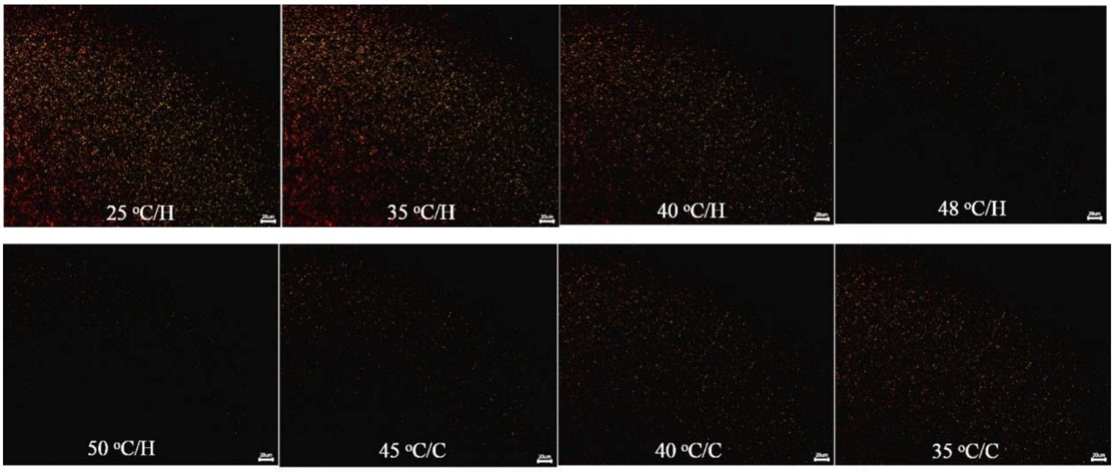

Figure S19. POM images of F_4H_7(I)MH_7(I) at different temperatures.

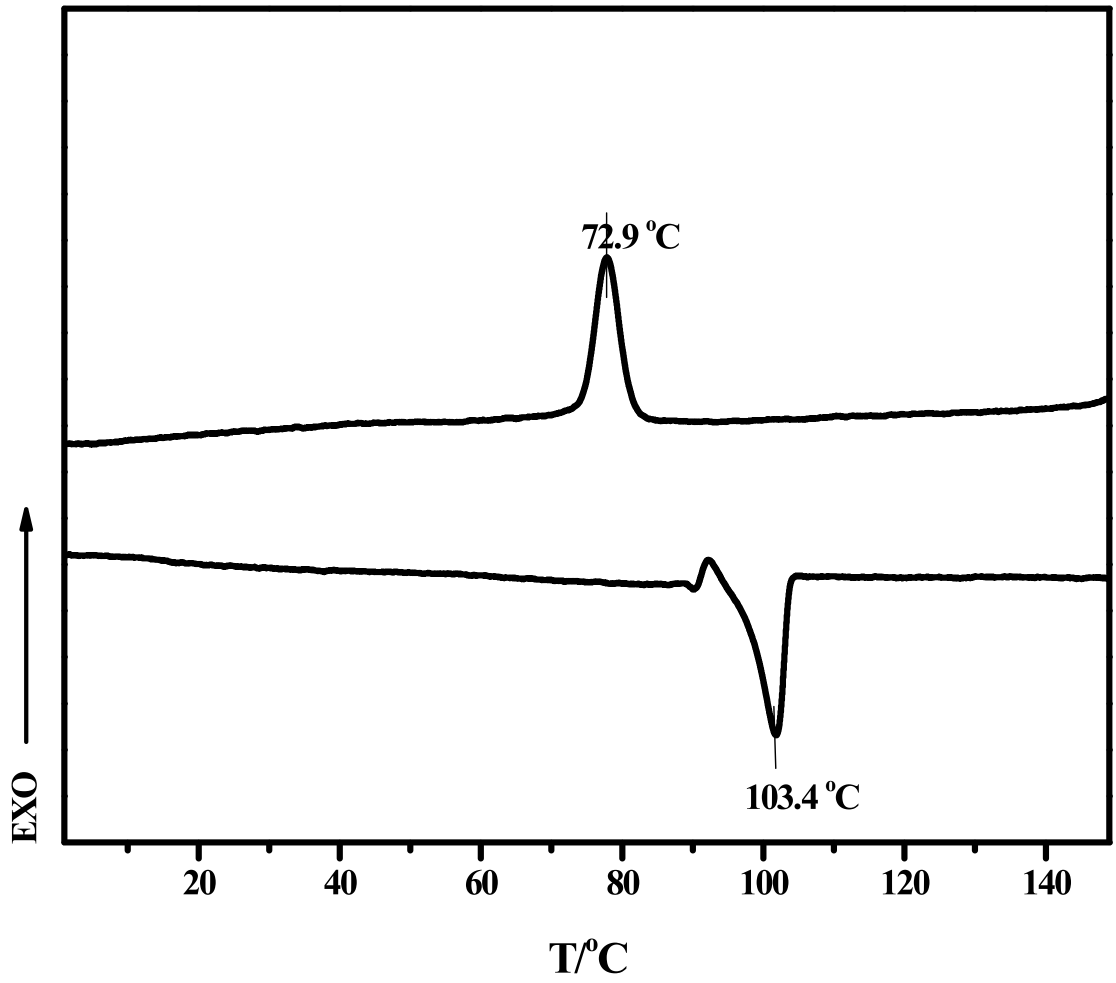

Figure S20. DSC curve of $F_6H_7(I)MH_7(I)$ obtained at a heating/cooling scanning rate of 1 °C min^{-1}.

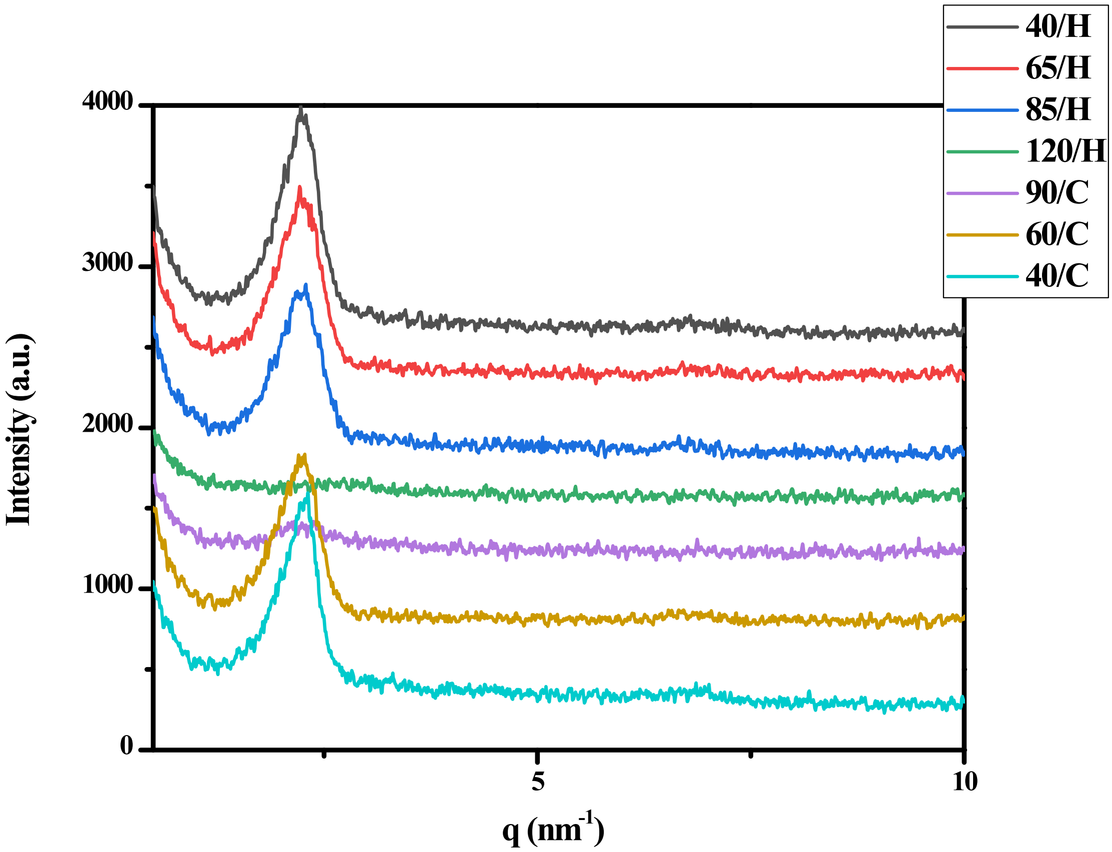

Figure S21. SAXS spectra of $F_6H_7(I)MH_7(I)$ at different temperatures after being annealed.

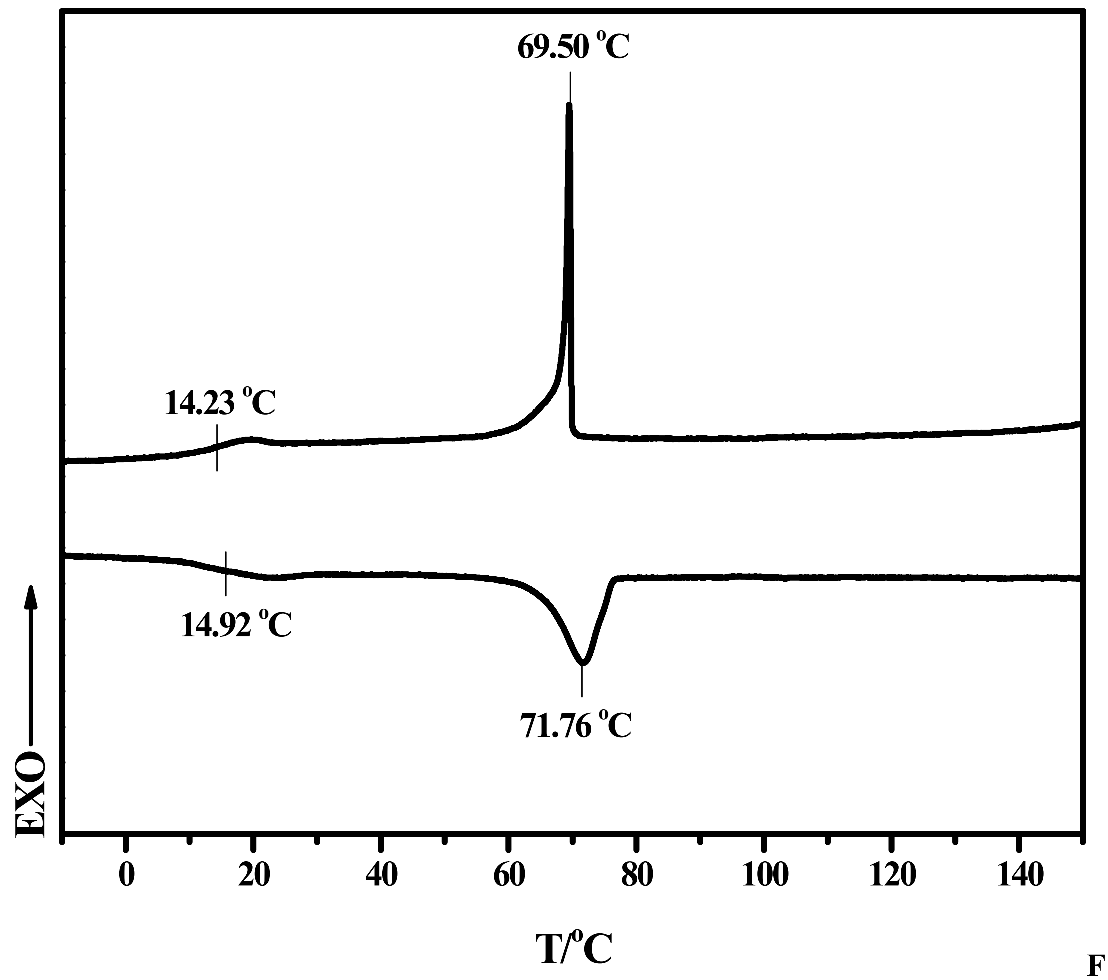

Figure S22. DSC curve of $F_6H_8(I)MH_8(I)$ obtained at a heating/cooling scanning rate of 1 °C min^{-1}.

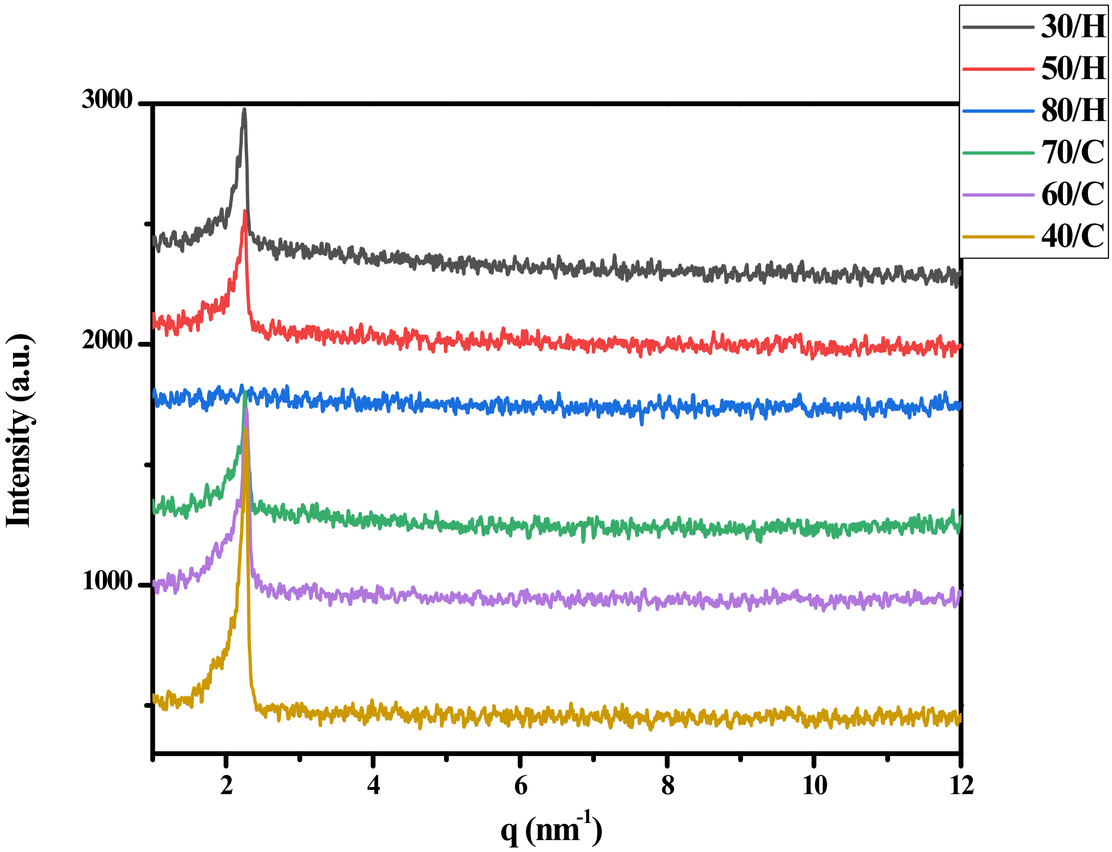

Figure S23. SAXS spectra of $F_6H_8(I)MH_8(I)$ at different temperatures after being annealed.

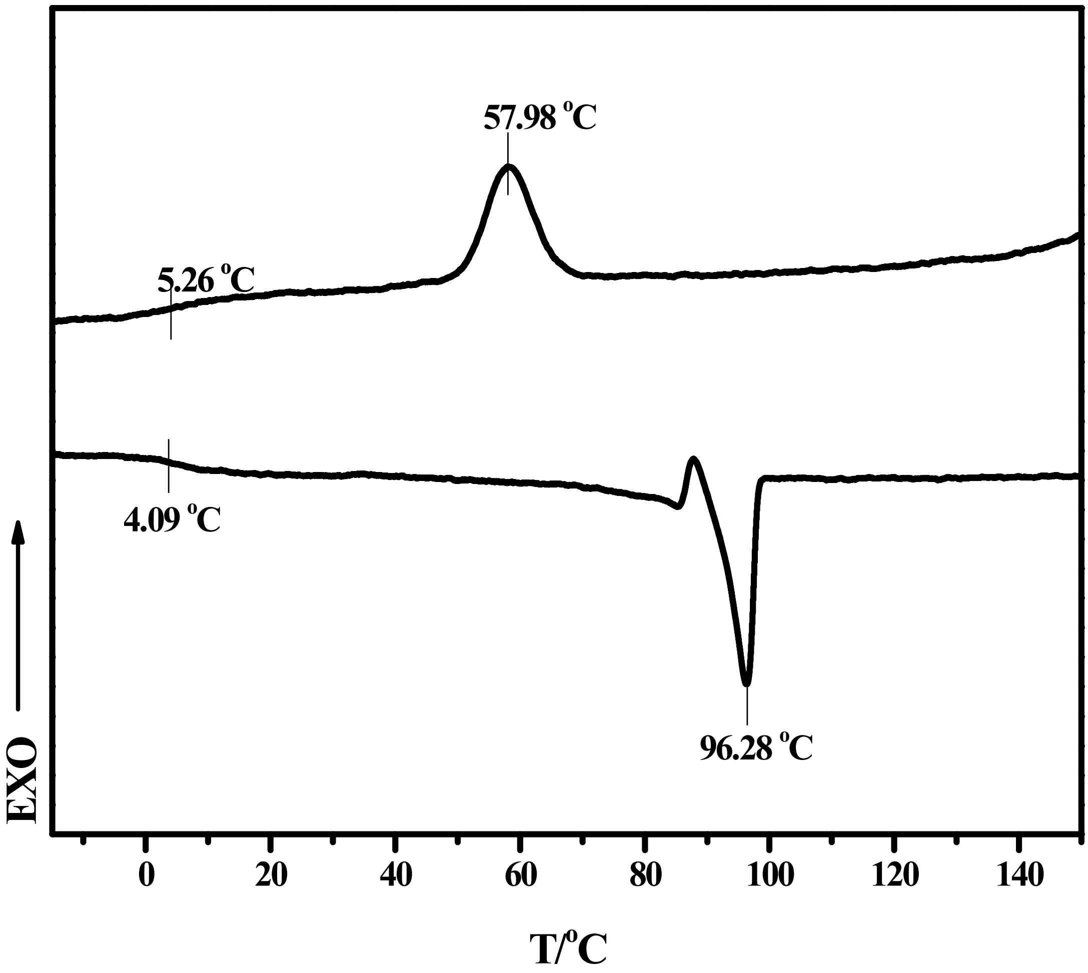

Figure S24. DSC curve of $F_6H_9(I)MH_9(I)$ obtained at a heating/cooling scanning rate of 1 °C min^{-1}.

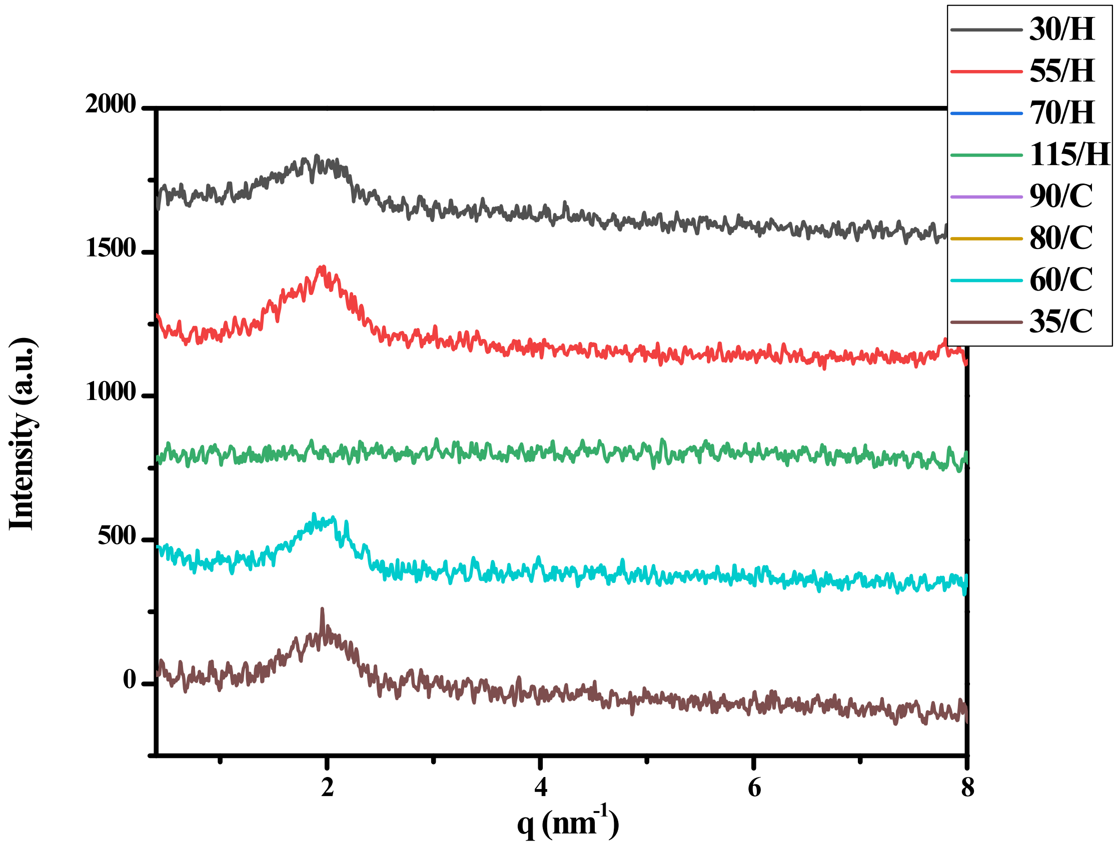

Figure S25. SAXS spectra of F_6H_9(I)MH_9(I) at different temperatures after being annealed.

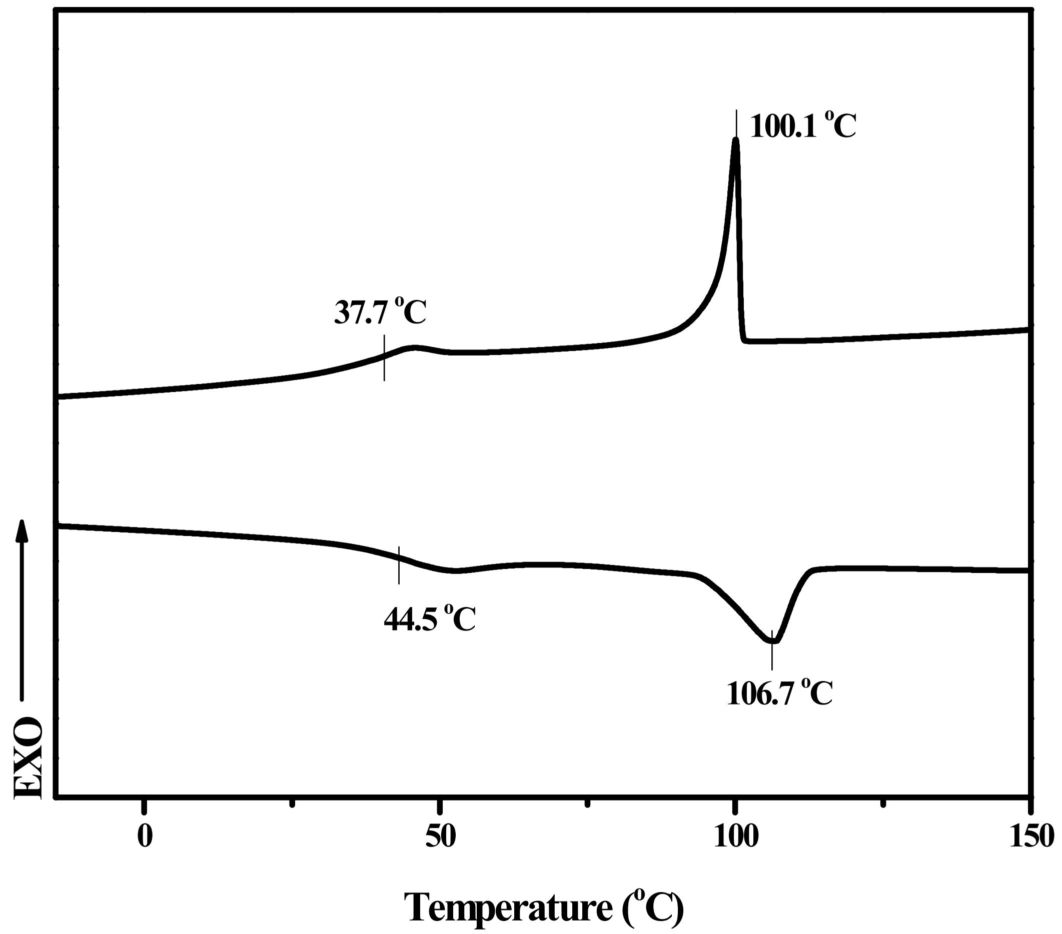

Figure S26. DSC curve of $F_8H_6(I)MH_6(I)$ obtained at a heating/cooling scanning rate of 10 °C min^{-1}.

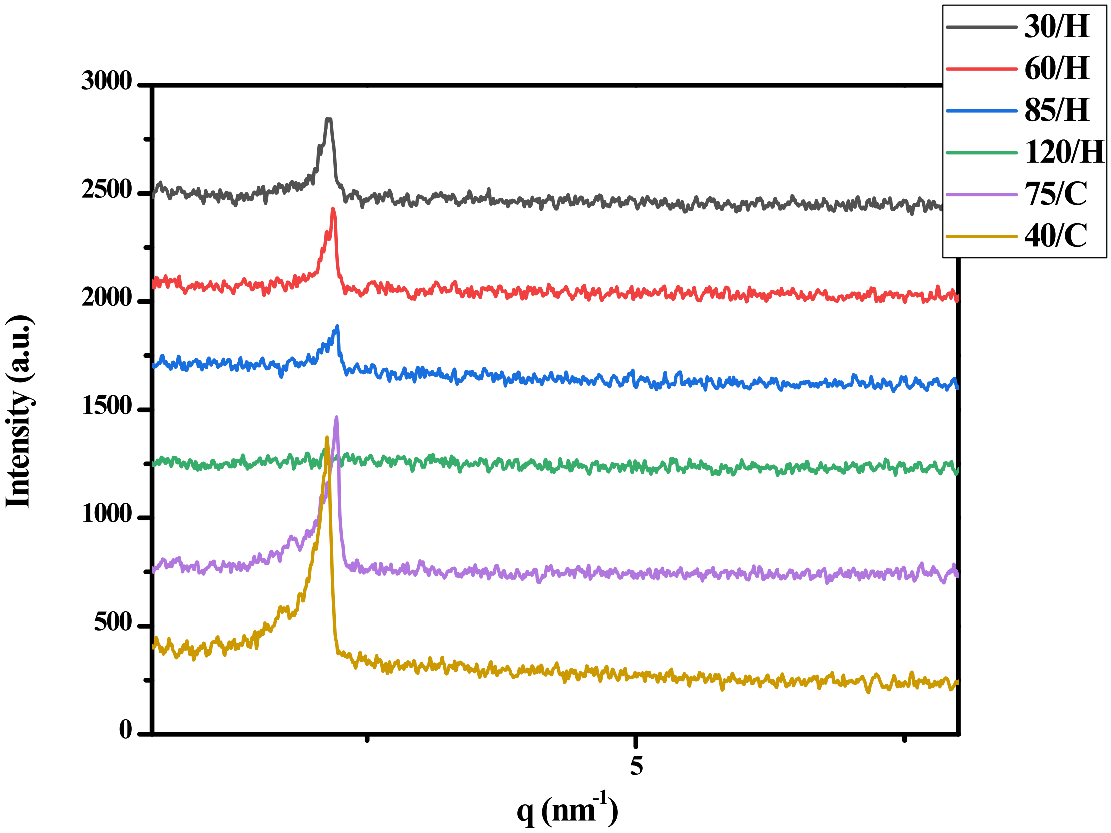

Figure S27. SAXS spectra of $F_8H_6(I)MH_6(I)$ at different temperatures after being annealed.

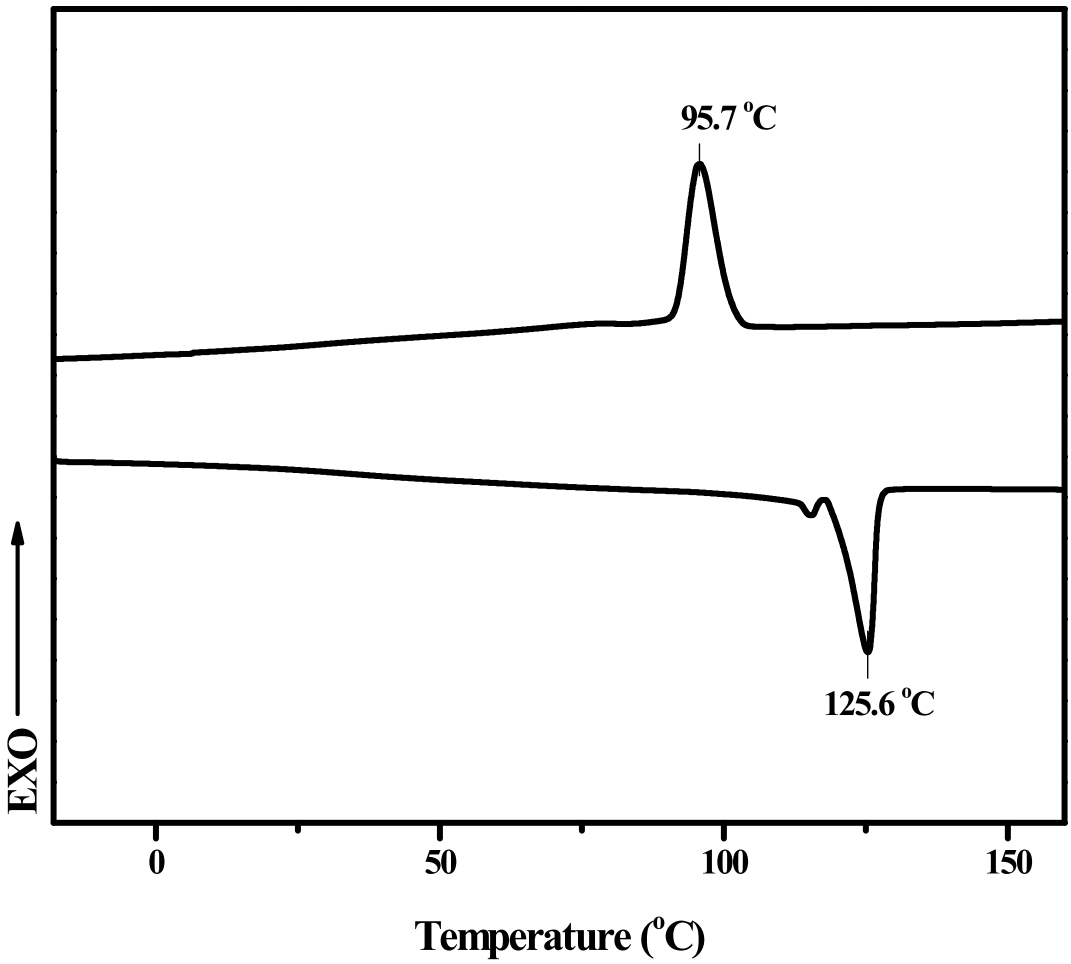

Figure S28. DSC curve of $F_8H_7(I)MH_7(I)$ obtained at a heating/cooling scanning rate of 10 °C min^{-1}.

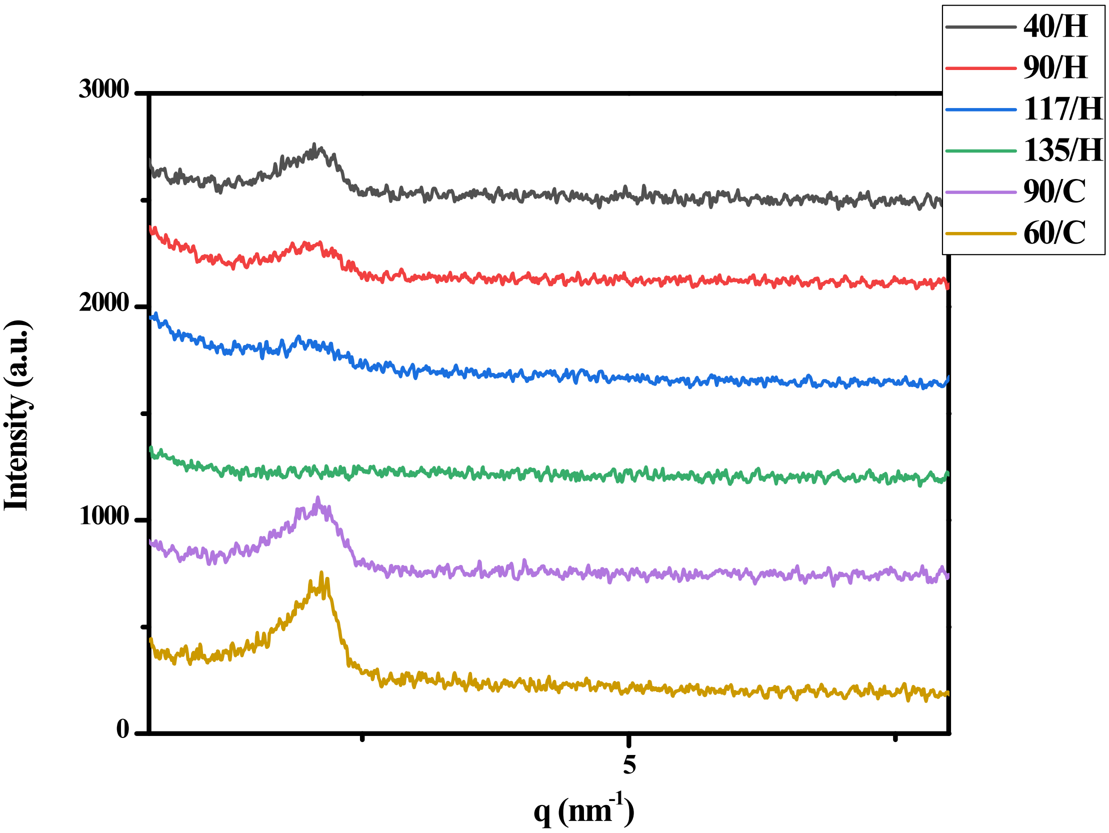

Figure S29. SAXS spectra of $F_8H_7(I)MH_7(I)$ at different temperatures after being annealed.

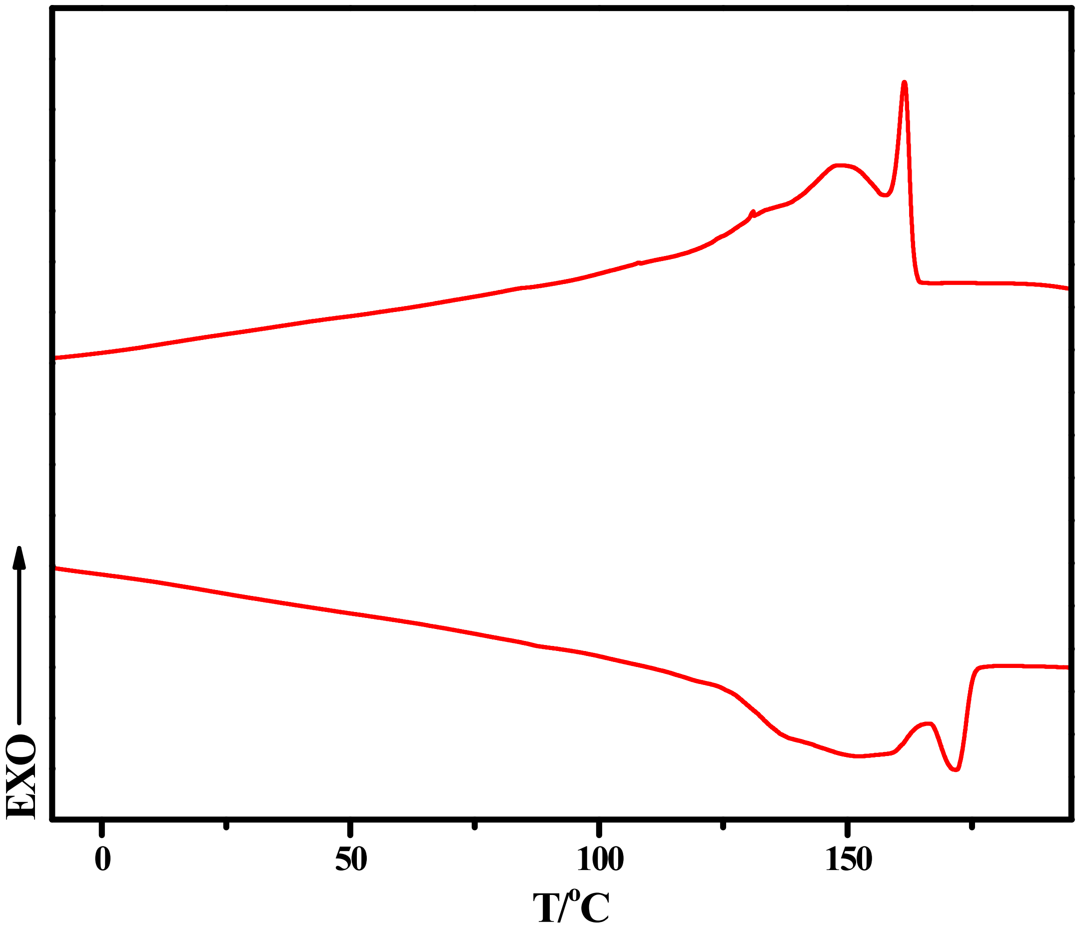

Figure S30. DSC curves of $F_4H_6MH_6$ obtained at heating/cooling scanning rate of 10 °C min^{-1}.

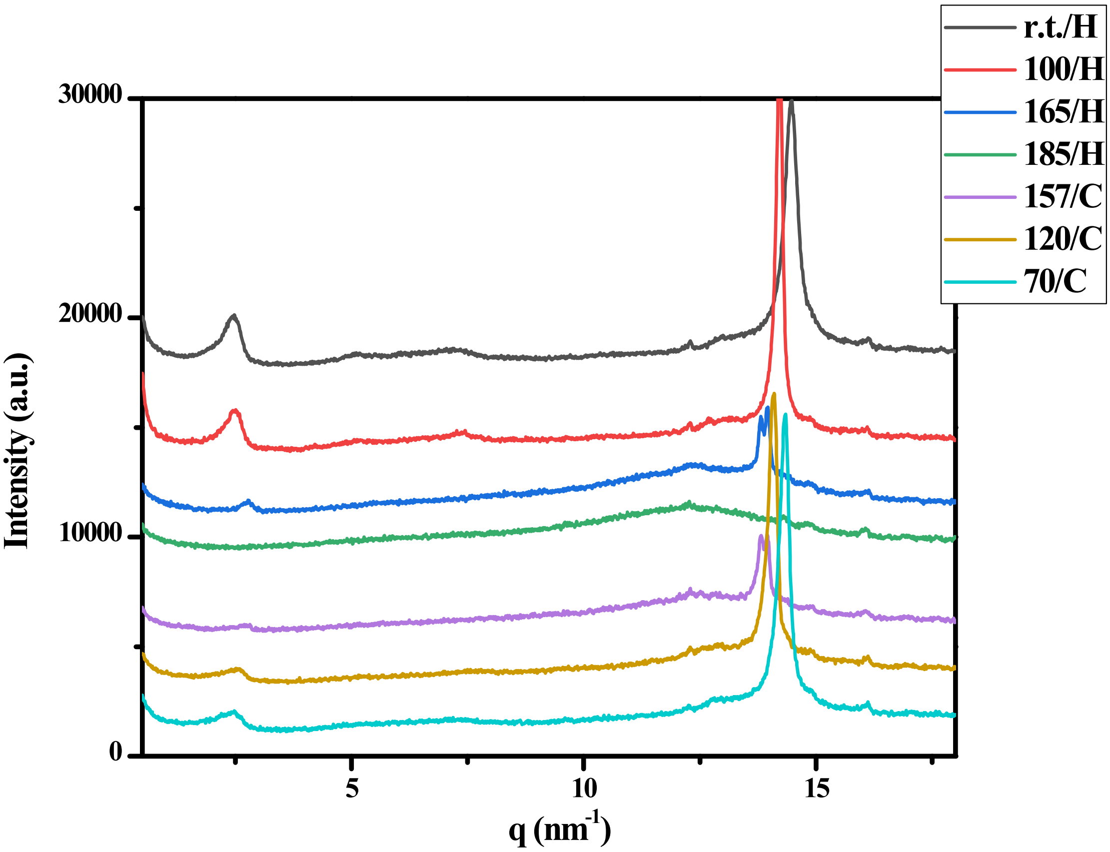

Figure S31. SAXS spectra of $F_4H_6MH_6$ at different temperatures after being annealed.

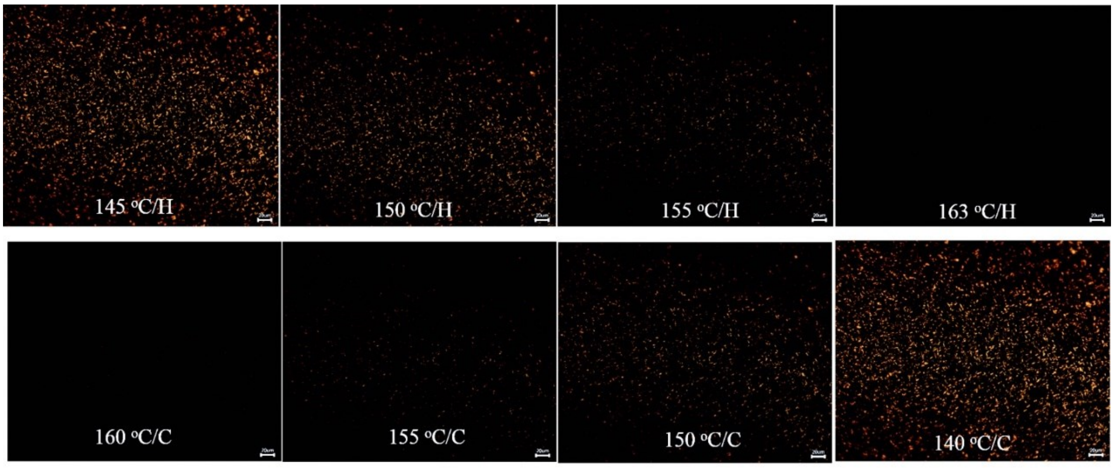

Figure S32. POM images of $F_4H_6MH_6$ at different temperatures.

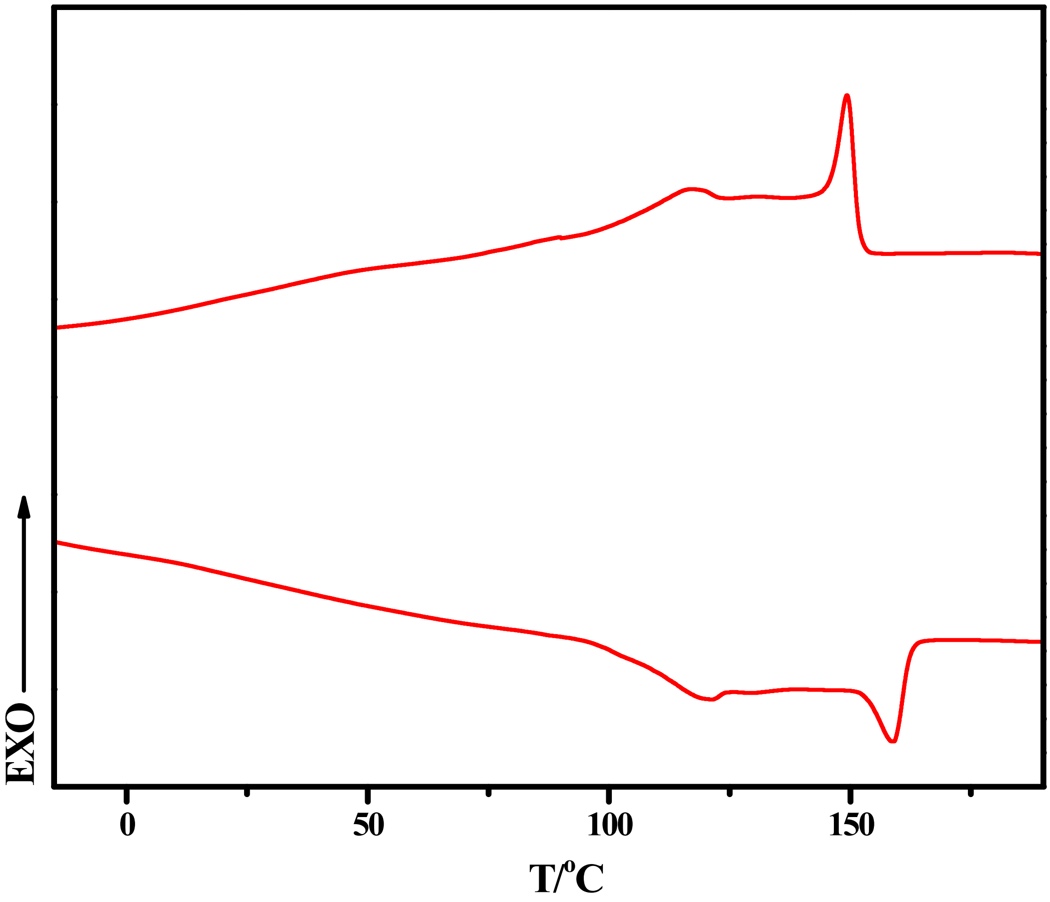

Figure S33. DSC curve of $F_4H_7MH_7$ obtained at a heating/cooling scanning rate of 10 ^{o}C min^{-1}.

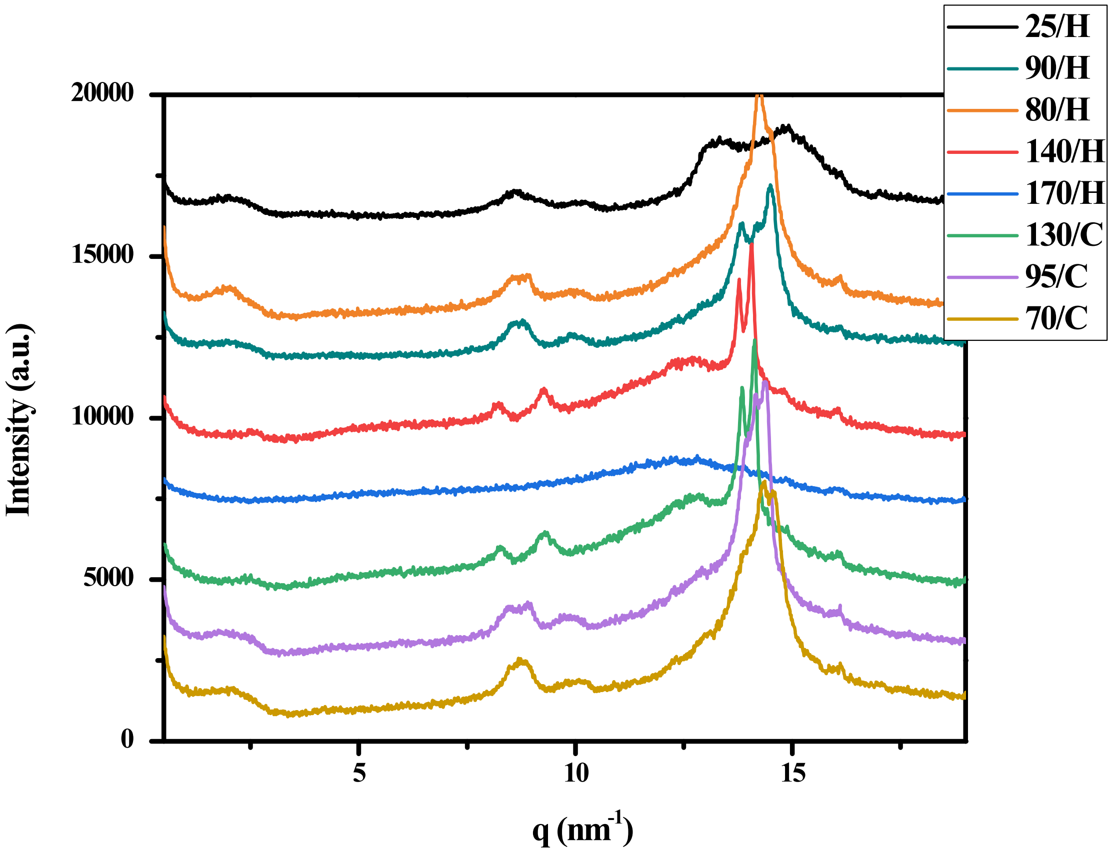

Figure S34. SAXS spectra of $F_4H_7MH_7$ at different temperatures after being annealed.

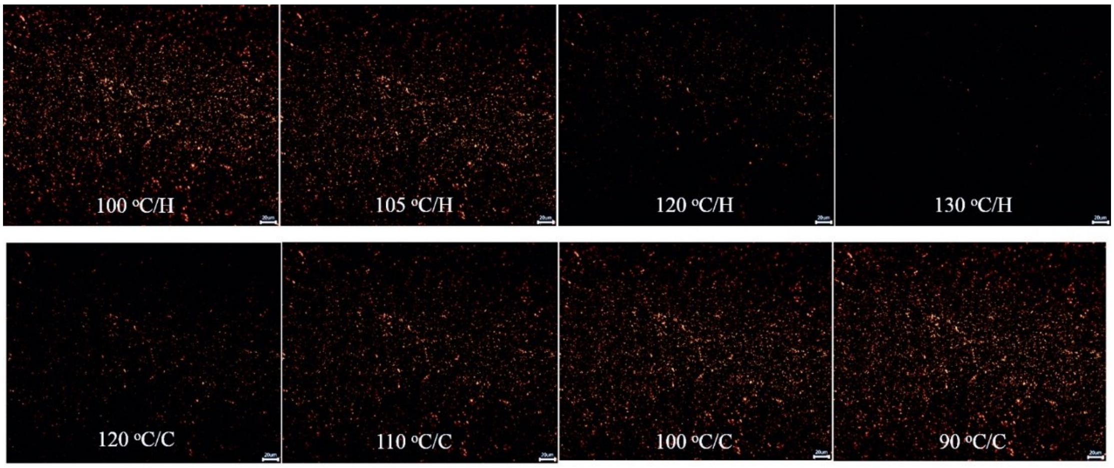

Figure S35. POM images of $F_4H_7MH_7$ at different temperatures.

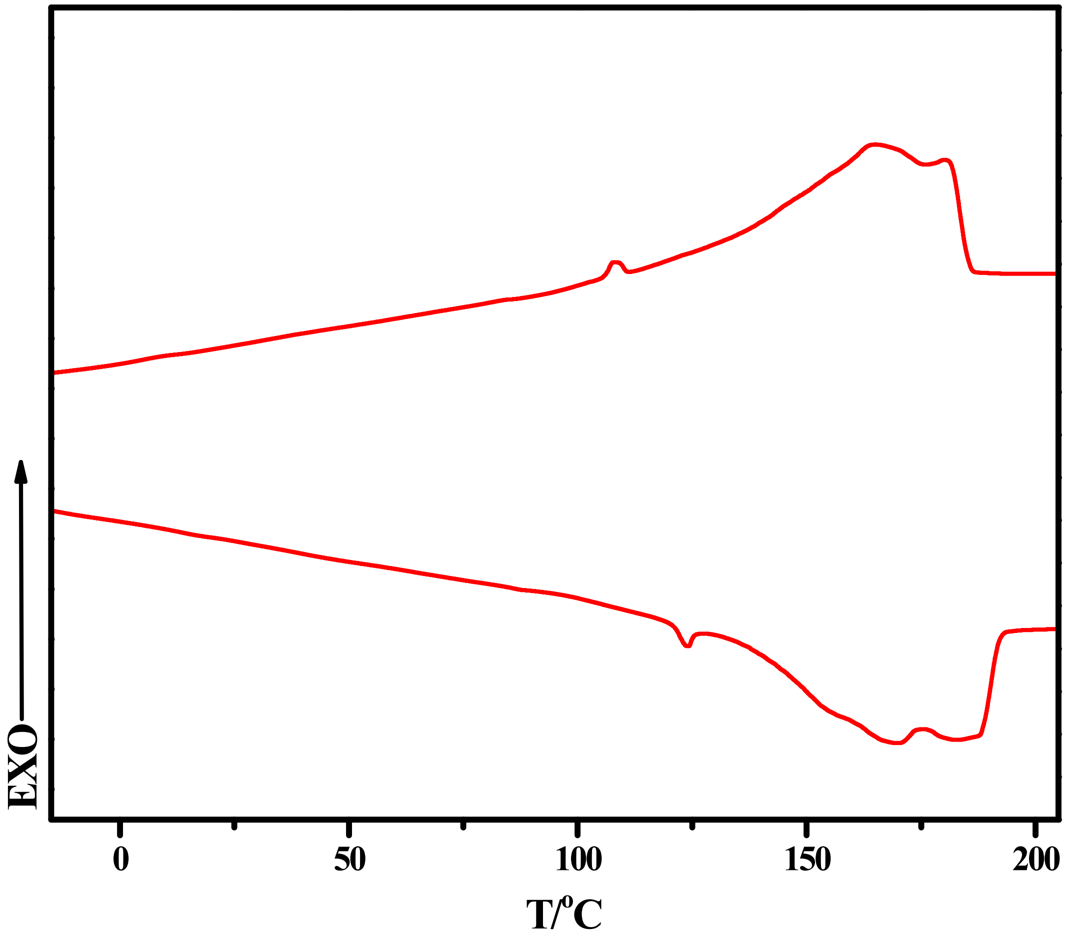

Figure S36. DSC curves of $F_6H_6MH_6$ obtained at heating/cooling scanning rate of 10 $^{o}C\ min^{-1}$.

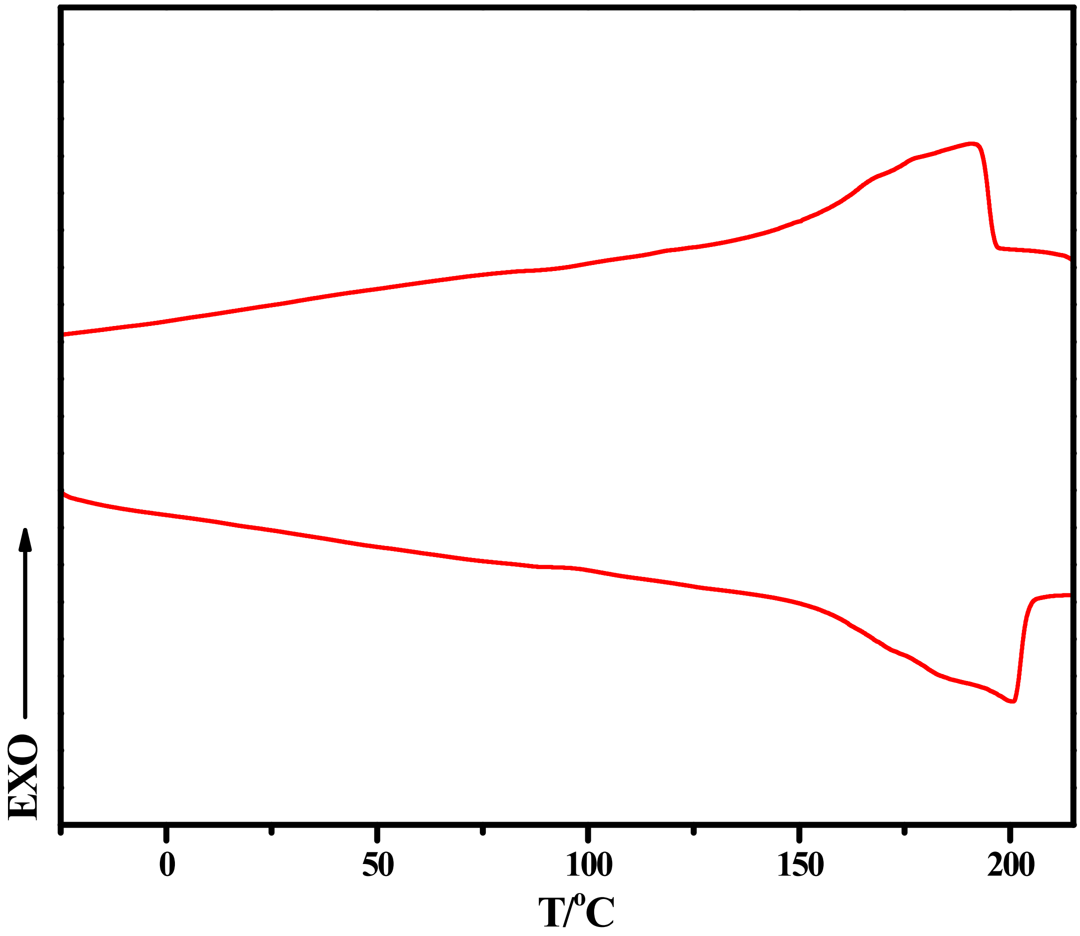

Figure S37. DSC curves of $F_8H_6MH_6$ obtained at heating/cooling scanning rate of 10 °C min^{-1}.

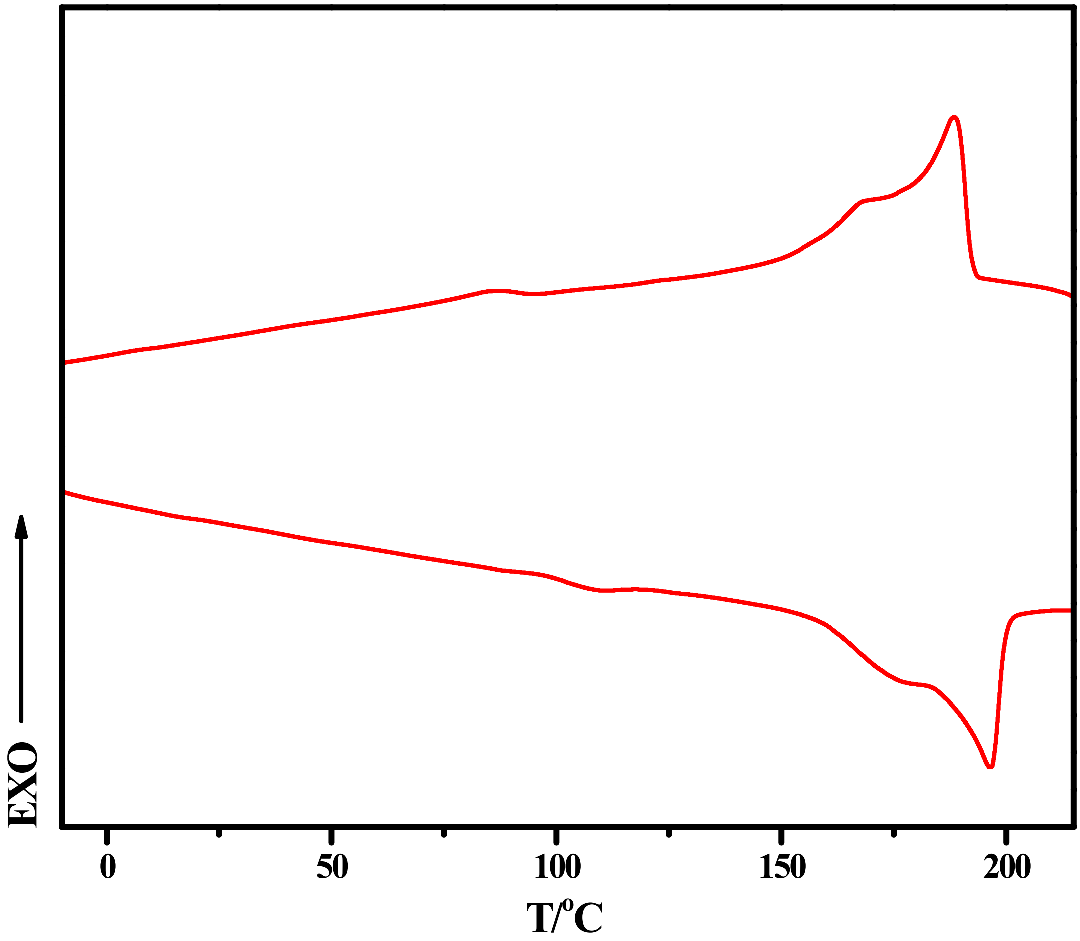

Figure S38. DSC curves of $F_8H_7MH_7$ obtained at heating/cooling scanning rate of 10 °C min^{-1}.

2. Lattice Parameter

Table S2. Indices (*hkl*) and *d*-spacings (observed and calculated from best fit lattice) of the diffraction peaks for the rectangular columnar phase observed at room temperature in $F_6H_7MH_7$

r.t./H	q**/nm^{-1}**	**h**	**k**	d_{cal}**/nm**	d_{obs}**/nm**
	1.89	1	0	3.33	3.32
	3.25	1	1	1.92	1.93
a = 3.84 nm	3.79	2	0	1.66	1.66
	4.28	2	1	1.26	1.47
	6.53	2	2	0.96	0.96
	7.79	4	0	0.83	0.81
	9.58	3	3	0.64	0.66

Table S3. Indices (*hkl*) and *d*-spacings (observed and calculated from best fit lattice) of the diffraction peaks for the rectangular columnar phase observed at 100 °C in $F_6H_7MH_7$

100/H	q**/nm^{-1}**	**h**	**k**	d_{cal}**/nm**	d_{obs}**/nm**
	2.05	1	0	3.07	3.07
	3.30	0	1	1.90	1.90
	3.84	1	1	1.62	1.64
a = 3.07 nm	4.11	2	0	1.54	1.53
b = 1.90 nm	6.62	0	2	0.95	0.95
	7.12	3	1	0.90	0.88
	7.76	2	2	0.81	0.81

Table S4. Indices (*hkl*) and *d*-spacings (observed and calculated from best fit lattice) of the diffraction peaks for the rectangular columnar phase observed at room temperature in $F_6H_6MH_6$

r.t./H	**q/nm^{-1}**	**h**	**k**	**d$_{calcd}$/nm**	**d$_{obs}$/nm**
	2.15	1	0	2.92	2.92
a = 2.92 nm	3.36	0	1	1.87	1.87
b = 1.87 nm	6.50	3	0	0.97	0.97
	7.03	1	2	0.89	0.89
	7.48	3	1	0.86	0.84
	7.81	2	2	0.79	0.80
	9.95	0	3	0.62	0.63
	10.29	1	3	0.61	0.61

Table S5. Indices (*hkl*) and *d*-spacings (observed and calculated from best fit lattice) of the diffraction peaks for the rectangular columnar phase observed at 175 °C in $F_6H_6MH_6$

175/H	**q/nm^{-1}**	**h**	**k**	**d$_{calcd}$/nm**	**d$_{obs}$/nm**
	3.29	1	0	1.91	1.91
a = 1.91 nm	6.63	2	0	0.96	0.95
	7.46	0	2	0.84	0.84
	9.58	3	0	0.64	0.66
b = 1.68 nm	10.15	2	2	0.63	0.62
	11.73	0	3	0.56	0.54

Table S6. Indices (*hkl*) and *d*-spacings (observed and calculated from best fit lattice) of the diffraction peaks for the rectangular columnar phase observed at 50 °C in $F_8H_7MH_7$

50/H	**q/nm^{-1}**	**h**	**k**	d_{cal}**/nm**	d_{obs}**/nm**
a = 3.86 nm	1.88	1	0	3.34	3.34
	3.21	1	1	1.93	1.96
	3.75	2	0	1.67	1.68
	6.50	2	2	0.97	0.97
	8.23	3	2	0.77	0.76
	9.94	3	3	0.64	0.63

3. Electron density reconstruction

Two-dimensional electron density maps could be reconstructed on the basis of the general formula:

$$\rho(xy) = \sum_{hk} F(hk)\exp[i2\pi(hx + ky)] \tag*{(1),}$$

here *F*(*hk*) is the structure factor of a diffraction peak with index (*hk*). The experimentally observed diffraction intensity

$$I(hk) = K \cdot F(hk) \cdot F^*(hk) = K \cdot \left|F(hk)\right|^2 \tag*{(2),}$$

here K is a constant related to the sample volume, incident beam intensity etc. In this paper we are only interested in the relative electron densities, hence this constant is simply taken to be 1. Thus the electron density is

$$\rho(xy) = \sum_{hk} \mathrm{sqrt}[I(hk)]\exp[i2\pi(hx + ky) + \varphi_{hk}] \qquad (3),$$

here ϕ_{hk} is the phase angle of the *hk* Bragg reflection.

As the observed diffraction intensity $I(hk)$ is only related to the amplitude of the structure factor $|F(hk)|$, the information about the phase of $F(hk)$, ϕ_{hk}, cannot be determined directly from experiment. However, the problem is significantly simplified with most space group symmetries, where the phase angle ϕ_{hk} of a given (hk) reflection has limited choices. In this work, the structures have *p*2*mm* or *p*6*mm* symmetry, which are centrosymmetric. Thus the phase angle ϕ_{hk} is limited to 0 or π.

Table S7. Experimental *d*-spacings, relative integrated intensities, and phases of the *p*2*mm* phase used in the reconstruction of $\rho(xy)$; all intensity values are Lorentz and multiplicity corrected.

(*hk*)	$d_{\text{obs.}}$ –spacing (nm)	*intensity* (Lorentz corrected)	*phase*
(10)	2.05	100	0
(01)	3.30	91.7	0
(11)	3.84	57.3	π
(20)	4.11	25.9	π
(02)	6.62	64.4	0
(31)	7.12	13.5	Π
(22)	7.76	42.9	0
	a = 3.07 nm, b = 1.90 nm		

Table S8. Experimental *d*-spacings, relative integrated intensities, and phases of the *p*6*mm* phase used in the reconstruction of $\rho(xy)$; all intensity values are Lorentz and multiplicity corrected.

(*hk*)	$d_{\text{obs.}}$ –spacing (nm)	*intensity* (Lorentz corrected)	*phase*
(10)	1.89	26.3	0
(11)	3.25	17.4	0
(20)	3.79	10.2	π
(22)	6.53	22.5	0
(40)	7.79	100	0
	a = 3.84 nm		